Journal of the Geological Society

Carboniferous appinitic intrusions from the northern North China craton: geochemistry, petrogenesis and tectonic implications

Xiaohui Zhang, Yanlong Gao, Zhijun Wang, Hu Liu and Yuguang Ma

Journal of the Geological Society 2012, v.169; p337-351.
doi: 10.1144/0016-76492011-062

Notes

Journal of the Geological Society, London, Vol. **169**, 2012, pp. 337–351. doi: 10.1144/0016-76492011-062.

Carboniferous appinitic intrusions from the northern North China craton: geochemistry, petrogenesis and tectonic implications

XIAOHUI ZHANG[1*], YANLONG GAO[2], ZHIJUN WANG[2], HU LIU[3] & YUGUANG MA[1]

[1]*State Key Laboratory of Lithospheric Evolution, Institute of Geology and Geophysics, Chinese Academy of Sciences, Beijing 100029, China*

[2]*Yangshan Gold Mine Corporation Limited, China National Gold Group, Yixian 746400, China*

[3]*Lanzhou University, Lanzhou 730000, China*

**Corresponding author (e-mail: zhangxh@mail.iggcas.ac.cn)*

Abstract: Laser ablation inductively coupled plasma mass spectrometry zircon U–Pb dating and geochemical study document Carboniferous (*c*. 320–317 Ma) appinitic intrusions from the northern North China craton. The rock suite mainly consists of hornblende diorites and monzodiorites, with an SiO_2 range from 46.8 to 55.4%. These rocks exhibit high alkali contents, strong enrichment in large ion lithophile elements and light rare earth elements, and depletion in high field strength elements, with radiogenic $^{87}Sr/^{86}Sr_i$ ratios of 0.7058–0.7093, unradiogenic $\varepsilon_{Nd}(t)$ of −9.3 to −13.9 and zircon $\varepsilon_{Hf}(t)$ from −8.5 to −18.4. These geochemical features suggest that their generation may involve a distinctive two-stage process: (1) a precursory metasomatism stage of mantle peridotites by melts from subduction-related sediments; (2) a delayed partial melting stage probably initiated by post-subduction transcurrent movements along pre-existing lithospheric shear zones. These mafic to intermediate intrusions, plus other coeval mafic– ultramafic complexes and high Ba–Sr granites from neighbouring regions, not only witness a heterogeneously enriched subcontinental lithospheric mantle along the northern North China craton, but also attest to a reworking-dominated metacratonic process within a post-subduction transtensional regime.

Supplementary material: Data on mineral composition, zircon dating and Hf isotopic composition are at http://www.geolsoc.org.uk/SUP18513.

Of all the mafic–ultramafic rocks associated with granites, the appinitic suite represents the most puzzling but may be the most edifying. After its introduction from the Appin district of Scotland (Bailey & Maufe 1916), the appinitic suite has been widely documented from various calc-alkaline granitoid batholiths worldwide (Ayrton 1991; Bowes & Košler 1993; Fowler & Henney 1996; Fowler *et al*. 2001, 2008; Atherton & Ghani 2002; Castro *et al*. 2003; Ye *et al*. 2008). It includes a wide variety of mafic rocks characterized by hydrous mineral assemblages of hornblende and biotite and by an overall andesitic to basaltic composition of calc-alkaline to shoshonitic affinity (Bowes & Košler 1993; Fowler & Henney 1996; Pitcher 1997; Fowler *et al*. 2001, 2008; Atherton & Ghani 2002; Castro *et al*. 2003). Of particular note is that it can be likened to the low-silica components from various sanukitoid suites worldwide (Stern *et al*. 1989; Kovalenko *et al*. 2005; Lobach-Zhuchenko *et al*. 2005; Heilimo *et al*. 2010; Qian & Hermann 2010). The appinitic suite is revealing in that (1) it commonly forms the mafic precursors of granitoid batholiths and thus testifies to mantle involvement in granite genesis (Fowler & Henney 1996; Pitcher 1997; Bea *et al*. 1999; Fowler *et al*. 2001, 2008; Atherton & Ghani 2002; Castro *et al*. 2003), and (2) it is generally characteristic of the final stage of orogeny and even indicative of critical post-subduction events such as slab break-off or delamination (Atherton & Ghani 2002; Kovalenko *et al*. 2005; Ye *et al*. 2008; Heilimo *et al*. 2010). Therefore, constraining the origin and tectonic affiliation of appinitic suites can be of much help not only in providing important clues to sources of orogenic magmas, but also in understanding the tectonic evolution of ancient convergent plate margins.

The northern North China craton has been a convergent plate margin during Palaeozoic times, mainly in response to multiple orogenic cycles associated with the closing of the Palaeo-Asian Ocean in the Central Asian Orogenic Belt. This resulted in several episodes of Palaeozoic magmatism in the region (Zhang & Zhai 2010, and references therein). It is clear that resolving this prolonged convergent history requires our understanding of the tectonic affiliation of these magmatic events with corresponding orogenic processes in the Central Asian Orogenic Belt.

In this contribution, we present new laser ablation inductively coupled plasma mass spectrometry (LA-ICP-MS) zircon U–Pb age, whole-rock geochemistry and Sr–Nd isotopes, and *in situ* zircon Hf isotopic compositions for the Carboniferous mafic to intermediate intrusive rocks from southern Inner Mongolia along the northern North China craton to: (1) document the geochemical characteristics of these rocks; (2) trace their magma sources and constrain their petrogenesis; (3) probe the tectonic environment in which they evolved.

Geological background

With the Central Asian Orogenic Belt on the north and the Qinling–Dabie–Sulu Orogenic Belt on the south, the North China craton comprises two Archaean continental blocks (Eastern and Western) separated by a Proterozoic Trans-North China Orogenic Belt (Zhao *et al*. 2001) (Fig. 1a). The Eastern and Western blocks developed independently from late Archaean to early Palaeoproterozoic time and collided to form a coherent craton at *c*. 1.85 Ga (Zhao *et al*. 2001). The craton features a basement of dominantly Archaean to Palaeoproterozoic tonalitic–trondhjemitic–granodioritic (TTG) gneisses and metavolcanic and metasedimentary rocks. Subsequent covers include

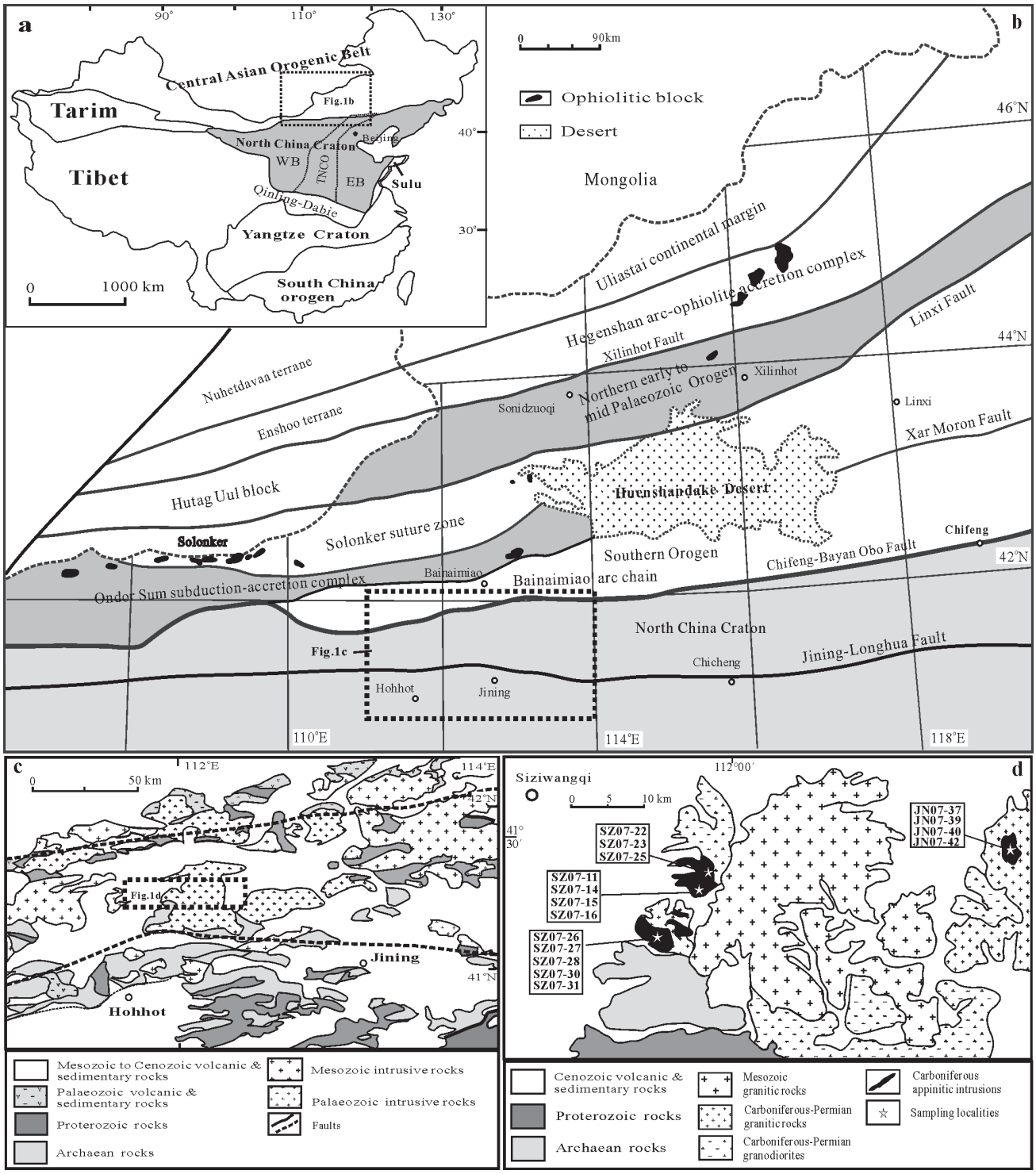

Fig. 1. (**a**) Major tectonic divisions of China. Also shown are the subdivisions of the North China craton (Zhao *et al*. 2001). EB, Eastern block; TNCO, Trans-North China orogen; WB, Western block. Rectangle marks area of (**b**). (**b**) Tectonic framework of Central and South Inner Mongolia (modified from Jian *et al*. 2008). Rectangle marks area of (**c**). (**c**) Sketch geological map of south Inner Mongolia (modified from Ma 2002). (**d**) Sketch geological map of the Siziwangqi appinitic intrusions (modified from IMBGMR 1972, 1975), with the sample locations shown.

the Mesoproterozoic clastic sedimentary succession of the Changcheng System, Cambrian to middle Ordovician marine sedimentary rocks, Carboniferous–Permian continental clastic rocks and Mesozoic basin deposits (Zhao *et al*. 2001; Kusky *et al*. 2007).

With a roughly east–west trend, the Central Asian Orogenic Belt consists of island arcs, ophiolites, oceanic islands, accretionary wedges, oceanic plateaux and micro-continents (Xiao *et al*. 2003; Windley *et al*. 2007). The northern China–Mongolia tract covers a vast area from southern Mongolia to northern China along the

middle–eastern segment of this orogenic belt, with the Solonker suture zone being its most prominent tectonic feature. This zone separates two opposite-facing continental blocks and is generally regarded to mark the final closure of the Palaeo-Asian Ocean (Fig. 1b) (Jian *et al*. 2008, 2010). The northern block includes the Hutag Uul terrane of South Mongolia (Badarch *et al*. 2002) and the northern orogen (early to mid-Palaeozoic) in northern China (Jian *et al*. 2008). The southern block comprises the southern orogen (early to mid-Palaeozoic) and the northern margin of the North China craton (Jian *et al*. 2010), with the Chifeng–Bayan Obo fault as the boundary between two units.

To the north of the fault lie the Bainaimiao arc chain and the Ondor Sum subduction–accretion complex, both forming an elongate, nearly east–west-trending belt (Wang *et al*. 1991; Xiao *et al*. 2003). The former mainly contains calc-alkaline tholeiitic basalts to minor felsic lavas, alkaline basalts, agglomerates, volcanic breccias and tuffs, as well as gabbros, granodiorites and granites (Jian *et al*. 2010). The latter is dominated by undeformed pillow basalts, calc-alkaline volcanic rocks and mylonitic metacherts from south to north at its type locality in the Ulan valley (Xiao *et al*. 2003; de Jong *et al*. 2006).

During late Palaeozoic to early Mesozoic time, the northern North China craton experienced several magmatic events (Zhang & Zhai 2010, and references therein), resulting in a Middle Devonian mafic–ultramafic complex (Zhang *et al*. 2009*a*) and alkaline intrusions (Zhang *et al*. 2010*a*), Carboniferous foliated calc-alkaline plutons (Zhang *et al*. 2007, 2009*b*), Early Permian high-K calc-alkaline I- and A-type granitoids (Zhang & Zhai 2010; Zhang *et al*. 2011*a*), and latest Permian to Early Triassic high-K calc-alkaline to alkaline intrusive rocks (Zhang *et al*. 2009*b*, 2010*b*).

The Siziwangqi region of southern Inner Mongolia is situated along the western segment of the northern North China craton (Fig. 1c). It features a Precambrian basement and Phanerozoic tectonic–magmatic events typical of the North China craton. The basement contains the lower amphibolite- to granulite-facies Archaean grey tonalitic gneisses and greenstones of the Jining group and the late Palaeoproterozoic low-grade metamorphic to unmetamorphosed rock sequences of the Zhaertai and Bayan Obo groups. The latter have a deposition time of *c*. 1750 Ma and are commonly interpreted to result from late Palaeoproterozoic rift after cratonization of the North China craton at *c*. 1.85 Ga (Li *et al*. 2007). Late Carboniferous to early Permian volcano-sedimentary sequences sporadically crop out in the northern part of the region and extend into the neighbouring orogenic belt. Jurassic to Cretaceous continental sedimentary rocks are present primarily in basins developed unconformably on the Precambrian basements.

Multiple phases of Phanerozoic igneous rocks intrude the Archaean and Palaeoproterozoic metamorphic rocks in the region. However, they are not well constrained up to now owing to few precise geochronological data. Based on field intrusive relations and petrography (IMBGMR 1972, 1975), they appear to occur in three episodes: the Caledonian (Early Palaeozoic), Hercynian (Late Palaeozoic) and Indonisian (Triassic) to Yanshannian (Jurassic and Cretaceous). The Caledonian suite is represented by a few strongly deformed dioritic stocks and enclaves with nearly east–west-trending foliation. The Hercynian suite consists of earlier minor phases of alkaline complexes with an age of *c*. 410 Ma (Zhang *et al*. 2010*a*) and mafic to intermediate intrusions, and later major phases of granodiorite–granite batholith formation. The Indonisian to Yanshannian suite comprises a few granitoid batholiths and numerous granite porphyritic dykes. These Phanerozoic igneous rocks were then covered by Cenozoic flood basalts and sediments.

Analytical methods

Major element compositions of minerals were measured on a JEOL JXA-8100 electron microprobe at the Institute of Geology and Geophysics, Chinese Academy of Sciences (IGGCAS). The operating conditions were 15 kV accelerating voltage, 10 nA beam current and 3 μm spot diameter. Well-defined natural mineral standards were applied for calibration. The analytical errors are generally less than 2%.

Zircons were separated from representative rock samples using standard density and magnetic separation techniques and purified by handpicking under a binocular microscope. Cathodoluminescence (CL) images were obtained for zircons prior to analyses, using a JXA-8100 microprobe at IGGCAS to reveal their internal structures.

Zircons were dated by ICP-MS using an Agilent 7500a system equipped with a 193 nm laser, housed at the State Key Laboratory of Geological Processes and Mineral Resources, China University of Geosciences in Wuhan, China. Harvard zircon 91500 was used as a standard and the standard silicate glass NIST as the reference material. The spot diameter was 30 μm. The detailed analytical technique is similar to that described by Liu *et al*. (2010). The common-Pb corrections were made using the method of Anderson (2002) and the data were processed using the GLITTER (Griffin *et al*. 2008) and ISOPLOT (Ludwig 2001) programs.

Fresh rock samples were ground in an agate mill to *c*. 200 μm mesh powder for geochemical analyses. For major element determination, mixtures of whole-rock powder (0.5 g) and $Li_2B_4O_7 + LiBO_2$ (5 g) were heated and fused into glass discs and analysed by X-ray fluorescence spectroscopy (XRF) with a Shimadzu XRF 1500 sequential spectrometer at the IGGCAS. The analytical uncertainties are better than 5% as revealed by long-term measurements of Chinese national standards GSR-1 (granite) and GSR-3 (basalt). Loss on ignition was measured as the weight loss of the samples after 1 h heating under a constant temperature at 1000 °C.

Trace element abundances were obtained by ICP-MS on a VG-PQII system also at the IGGCAS. Samples were dissolved in distilled $HF + HNO_3$ in 15 ml high-pressure Teflon bombs at 120 °C for 6 days, dried and then diluted with 1% HNO_3 to 50 ml for analysis. A blank solution was prepared and the total procedural blank was <50 ng for all trace elements. Indium was used as an internal standard to correct for matrix effects and instrument drift. Precision for all trace elements is estimated to be 5% and accuracy is better than 5% for most elements, monitored by analyses of Chinese national standard samples GSR-1 and GSR-3.

Whole-rock Sr and Nd isotopic compositions were measured on a Finnigan Mat 262 thermal ionization mass spectrometer at the IGGCAS, following the procedure described by Zhang *et al*. (2008). Procedural blanks were <100 pg for Sm and Nd and <500 pg for Rb and Sr. $^{143}Nd/^{144}Nd$ was corrected for mass fractionation by normalization to $^{146}Nd/^{144}Nd = 0.7219$, and $^{87}Sr/^{86}Sr$ ratios were normalized to $^{86}Sr/^{88}Sr = 0.1194$. The measured values for the BCR-2 Nd standard and BCR-2 Sr standard were $^{143}Nd/^{144}Nd = 0.512641 \pm 0.000010$ (2σ, $n = 4$) and $^{87}Sr/^{86}Sr = 0.705018 \pm 0.000011$ (2σ, $n = 4$) during the period of data acquisition.

In situ zircon Hf isotopic analyses were conducted by multicollector (MC)-ICP-M using the Neptune S system, equipped with a 193 nm laser at the IGGCAS. Spot size of 32 μm was used for analysis, with a laser repetition rate of 10 Hz at 100 mJ. The detailed analytical procedure and correction for interferences follow those described by Wu *et al*. (2006). The $^{176}Hf/^{177}Hf$ and $^{176}Lu/^{177}Hf$ ratios of the standard zircon (91,500) during analysis were 0.282270 ± 0.000023 (2σ, $n = 15$) and 0.00028, similar to the

commonly accepted $^{176}Hf/^{177}Hf$ ratio of 0.282284 ± 0.000003 (1σ) measured using the solution method (Woodhead *et al*. 2004).

Field relations and petrography

The Hercynian mafic to intermediate complexes are located *c*. 30–80 km to the SE of Siziwangqi town (Fig. 1d). They occur either as small stocks intruding the Archaean gneisses or as xenoliths hosted in the Hercynian granodioritic to granitic rocks (IMBGMR 1972, 1975). However, contacts between the complexes and the Archaean basement are not exposed because of cover by Cenozoic sediments (Fig. 1d). The complexes have been intruded by slightly younger granites and feldspathic veinlets.

The rocks commonly have modal mineralogies of hornblende diorite, diorite and monzodiorite, with fine- to medium-grained intergranular textures. Hornblende diorites, with more than 75% amphibole, commonly occur as small blocks surrounded by massive diorite and monzodiorite. The most common medium-grained diorites typically comprise euhedral to subhedral amphibole (45–50%) and plagioclase (40–50%), and subhedral to anhedral biotite (3–10%). Accessory phases (<2%) include euhedral to subhedral apatite, subhedral zircon, euhedral titanite and magnetite, Amphiboles show a wide range of X_{Mg} (= Mg/(Mg + Fe*); 0.44–0.67) and are classified as Mg-hornblende and actinolite (Leake *et al*. 1997). They are locally altered to chlorite and epidote. Plagioclases generally have an andesite to albite composition ($An_{2-38}Ab_{60-98}Or_{0-2}$) and show mild to moderate sericitization. Flaky biotites are characterized by moderate Al contents and variable X_{Mg} of 0.44–0.56, with moderate chloritization.

With the amount of alkali feldspar increasing, diorites can grade into monzodiorites. Typical samples contain 45–60% plagioclase, 15–25% amphibole, 8–20% biotite, 5–12% alkali feldspar and 2–5% quartz, and accessory apatite, zircon and titanite. The textures and compositions of major constituents are similar to those of the diorite: green Mg-hornblende with X_{Mg} of 0.65–0.71, subhedral plagioclase ($An_{20-30}Ab_{70-80}$), anhedral alkali feldspar ($Or_{36-97}Ab_{3-55}An_{0-8}$), subhedral flaky biotite with X_{Mg} of 0.56–0.61.

Results

Zircon U–Pb data

Zircons from sample SZ07-15 are mostly subhedral, stubby to elongate prisms. They are about 80–220 μm long with length-to-width ratios between 2:1 and 5:1. In CL images, they commonly show low, homogeneous luminescence, with occasional oscillatory zoning (Fig. 2a). Twenty analyses on 20 grains yield U concentrations from 50 to 794 ppm, Th from 31 to 2031 ppm and Th/U ratios from 0.45 to 2.56. All spots define a weighted mean $^{206}Pb/^{238}U$ age of 320 ± 2 Ma with an MSWD of 2.9 (Fig. 2b).

Zircons from sample SZ07-26 are typically subhedral elongated crystals with 50–130 μm in size. Most grains display internal oscillatory zoning (Fig. 2c). Measured U concentrations from 16 analyses on 16 grains vary from 59 to 300 ppm and Th from 42 to 526 ppm. All analyses have Th/U ratios of 0.58–2.24 and yield a weighted mean $^{206}Pb/^{238}U$ age of 317 ± 3 Ma with an MSWD of 1.6 (Fig. 2d).

Zircons from sample JN07-37 are clear, euhedral to subhedral, stubby to elongate prisms, with a length from 60 to 180 μm and well-developed oscillatory zoning (Fig. 2e). Twenty-two measured grains yield U concentrations from 105 to 752 ppm and Th from 51 to 1906 ppm. All analyses have Th/U ratios from 0.6 to 2.54 and result in a weighted mean $^{206}Pb/^{238}U$ age of 319 ± 2 Ma with an MSWD of 1.7 (Fig. 2f).

Major oxides and trace elements

Major and trace element analyses are presented in Table 1. The rocks are basic to intermediate in composition (SiO_2 46.8–55.5%), with high contents of total Fe_2O_3 (6.76–11.47 %), K_2O (1.11–3.94%), CaO (4.81–9.39%) and TiO_2 (0.6%–1.70%), low P_2O_5 (0.14–0.79%), and varying abundances of MgO (3.63–11.38%), Al_2O_3 (10.59–19.74%), Cr (4–323 ppm) and Ni (25–167 ppm). Their Mg-numbers range from 43 to 69. In the total alkali v. silica plot (Le Maitre 2002) (Fig. 3a), the samples scatter in the fields of gabbro, gabbroic diorite, monzogabbro and monzodiorite. They exhibit a transitional character between medium- to high-K calc-alkaline and shoshonitic (Fig. 3b), with aluminum saturation index (ASI = molar $Al_2O_3/(CaO + K_2O + Na_2O)$) of 0.50–0.90.

In Figure 4, most samples roughly define a continuous evolution trend: SiO_2, CaO and Fe_2O_3* (total Fe as ferric iron) are positively correlated with MgO, whereas Al_2O_3, K_2O, Na_2O, TiO_2 and P_2O_5 are negatively correlated. Likewise, compatible elements such as Sc, Cr, Ni and V increase with increasing MgO, whereas Sr, Ba, Pb, Nb and Y decrease with increasing MgO. Th and Zr vary irregularly with increasing MgO. In addition, Cr is positively correlated with Ni (Fig. 4).

With respect to other trace elements, the rocks are characterized by moderate light rare earth element (LREE) enrichment (La_N/Yb_N = 7.33–38.5) and small negative Eu anomalies (Eu/Eu* = 0.86–1.0; Fig. 5a). In the primitive mantle (PM)-normalized trace element diagrams (Fig. 5b), they show enrichment in large ion lithophile elements (LILE, such as Sr, Ba, Rb) and LREE, but strong depletion in high field strength elements (HFSE) with pronounced Nb, Ta, P and Ti troughs.

Whole rock Sr–Nd and zircon Hf isotopic compositions

Whole-rock Sr–Nd isotope data, together with the calculated initial Sr–Nd isotopic compositions, are presented in Table 2. As shown in a plot of $\varepsilon_{Nd}(t)$ v. $^{87}Sr/^{86}Sr_i$ (Fig. 6), the rocks have initial $^{87}Sr/^{86}Sr$ ratios from 0.7058 to 0.7093 and moderately negative $\varepsilon_{Nd}(t)$ values from −9.92 to −13.40.

As presented in Figure 7, zircons from sample SZ07-15 show a range of initial $^{176}Hf/^{177}Hf$ ratios from 0.28205 to 0.28216 and $\varepsilon_{Hf}(t)$ values from −14.2 to −18.4, with crustal model ages of 2.24–2.49 Ga. Zircons from sample SZ07-26 exhibit a range of initial $^{176}Hf/^{177}Hf$ ratios from 0.28209 to 0.28238, $\varepsilon_{Hf}(t)$ from −8.5 to −17.1 and crustal model ages between 2.24 and 2.41 Ga. Zircons from sample JN07-37 display a range of initial $^{176}Hf/^{177}Hf$ ratios from 0.28218 to 0.28225, $\varepsilon_{Hf}(t)$ from −11.4 to −13.8 and model ages from 2.05 to 2.21 Ga.

Discussion

Petrogenesis

The well-defined zircon U–Pb ages presented in this study, plus a recently reported zircon U–Pb age of *c*. 330 Ma for a nearby dioritic stock (Zhou *et al*. 2009), firmly established an emplacement time of Carboniferous for the Hercynian mafic to intermediate complexes in the Siziwangqi region.

With their satellitic occurrence as small plutons or enclaves and hornblende-dominated mafic mineral character, the Siziwangqi rocks bear a remarkable resemblance to the appinite suite from the late Caledonian and late Variscan granitoid batholiths within Europe (Ayrton 1991; Bowes & Košler 1993; Fowler & Henney 1996; Fowler *et al*. 2001, 2008; Atherton & Ghani 2002; Castro

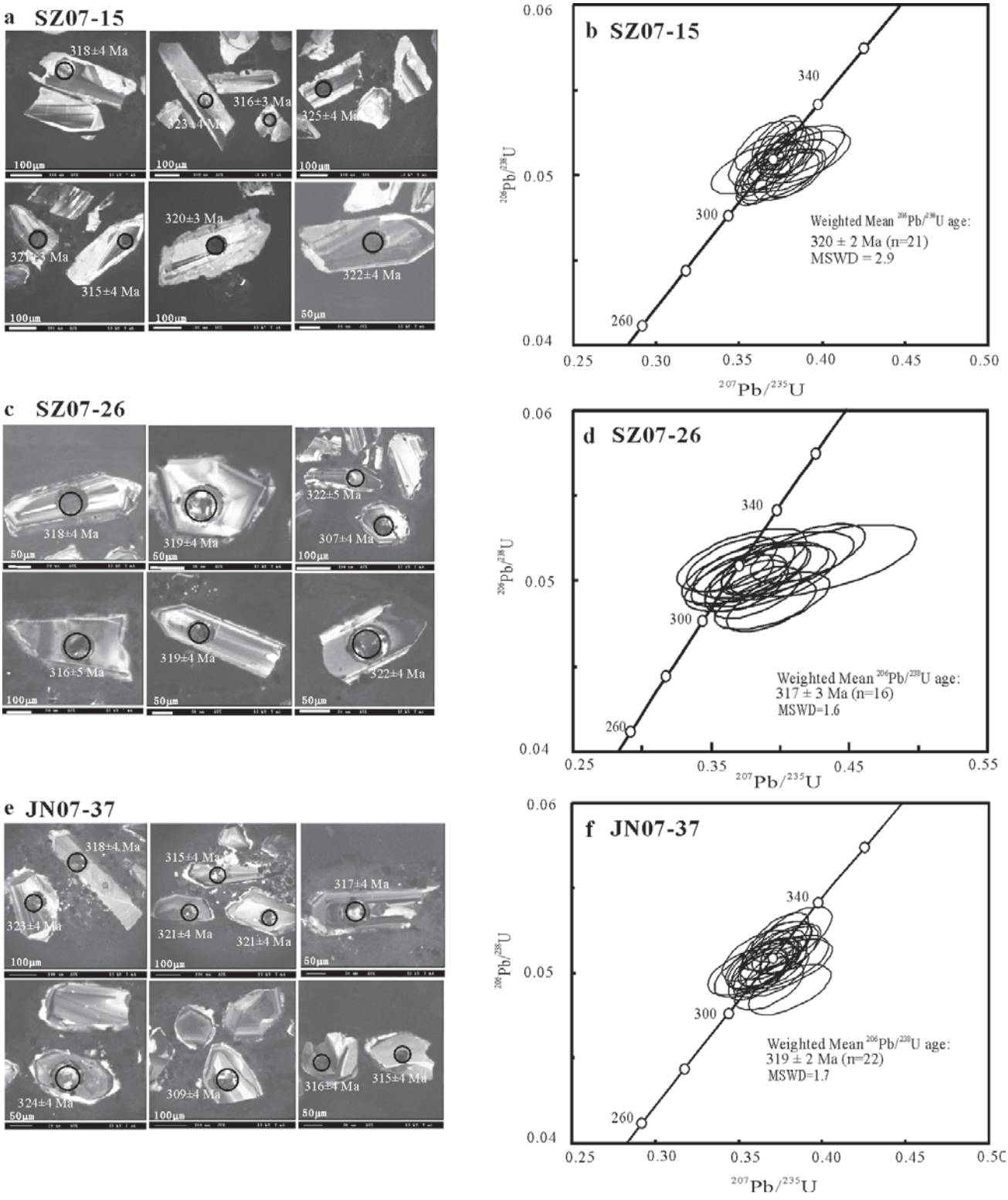

Fig. 2. (**a**, **c**, **e**) Cathodoluminescence (CL) images of the dated zircons and (**b**, **d**, **f**) zircon U–Pb concordia diagrams for samples SZ07-15, SZ07-26 and JN07-37 from the appinitic intrusions from southern Inner Mongolia.

et al. 2003). As in the case of these counterparts, the high-MgO content in many high-silica samples from the present rocks bestow a high-Mg andesitic affinity on them (Fig. 8). Furthermore, with their elevated alkali, Ba–Sr abundances and high LILE/HFSE and LREE/HFSE ratios, the Siziwangqi rocks are reminiscent of the low-silica counterparts from numerous sanukitoid suites worldwide (Kamei *et al*. 2004; Kovalenko *et al*. 2005; Tatsumi 2006; Heilimo *et al*. 2010; Qian & Hermann 2010).

Table 1. *Major and trace element data for the appinitic intrusions from southern Inner Mongolia*

Sample:	SZ07-11	SZ07-15	SZ07-16	SZ07-14	SZ07-22	SZ07-23	SZ07-25	SZ07-26
Rock type:	M.D	D	D	D	D	D	D	M.D
Longitude (E):	111°56.230′				111°57.697′			
Latitude (N):	41°25.387′				41°26.250′			
SiO_2	55.45	49.91	49.29	55.42	55.31	54.43	54.37	54.98
TiO_2	1.31	1.58	1.56	1.04	0.79	0.85	0.89	0.81
Al_2O_3	15.78	19.49	19.74	16.86	11.94	13.46	13.57	12.27
Fe_2O_3*	7.35	9.75	9.40	6.76	8.51	8.42	8.42	8.51
MnO	0.09	0.10	0.11	0.10	0.14	0.13	0.13	0.13
MgO	5.32	3.63	4.05	4.80	9.03	8.20	8.16	9.07
CaO	4.81	6.97	6.97	5.23	7.70	7.79	7.83	7.82
Na_2O	3.50	4.46	4.05	4.59	2.63	2.77	2.71	2.40
K_2O	3.94	2.17	2.33	2.95	1.75	1.73	1.83	1.78
P_2O_5	0.77	0.63	0.45	0.61	0.24	0.23	0.27	0.23
LOI	1.22	0.75	1.52	1.60	1.36	1.45	1.42	1.55
Total	99.54	99.44	99.47	99.97	99.40	99.47	99.59	99.55
Mg-no.	58.9	42.4	46.0	58.4	67.8	65.9	65.8	67.9
Sc	11.2	13.1	18.0	14.2	30.9	28.8	29.4	30.0
V	129.5	188	164	118	149	153	156	150
Cr	113	4.30	4.73	124	292	202	207	268
Co	24.5	24.5	25.8	20.6	36.2	36.2	35.5	36.7
Ni	66.4	27.8	15.0	71.9	167	152	157	190
Ga	20.5	25.1	23.0	18.8	14.1	16.0	16.8	15.1
Rb	106	47.8	76.4	73.8	41.2	74.5	66.3	50.6
Sr	1070	1343	1303	1172	512	709	689	598
Y	16.2	21.6	21.9	14.68	17.5	18.1	19.2	17.2
Zr	280	215	198	158	140	147	160	126
Nb	13.3	12.0	10.0	9.41	7.46	8.09	9.31	6.60
Cs	13.7	1.63	7.75	4.71	2.12	3.99	4.99	2.80
Ba	1722	117	1092	1617	592	737	796	720
Hf	7.28	5.26	4.69	4.01	3.75	3.88	4.21	3.47
Ta	0.62	0.34	0.45	0.57	0.40	0.52	0.67	0.35
Pb	15.4	12.2	10.3	14.5	9.24	12.9	11.9	10.0
Th	9.16	8.28	1.66	11.2	5.15	4.79	5.94	4.05
U	2.22	0.93	0.62	2.03	2.80	1.78	2.29	2.69
La	63.9	55.8	20.4	58.7	29.4	27.4	29.6	25.6
Ce	131	109	48.8	114	56.1	57.3	65.2	53.8
Pr	16.3	13.6	6.93	14.3	6.74	7.18	7.87	6.54
Nd	62.0	51.4	29.4	52.7	25.3	28.8	30.0	26.3
Sm	11.1	9.55	6.75	9.05	5.07	5.69	5.84	5.05
Eu	2.58	2.50	1.88	2.08	1.44	1.57	1.70	1.45
Gd	7.69	7.58	5.71	5.60	4.18	4.73	5.07	4.45
Tb	0.89	1.02	0.84	0.67	0.61	0.68	0.71	0.63
Dy	3.94	5.43	4.71	3.08	3.53	3.77	3.90	3.44
Ho	0.66	1.02	0.90	0.55	0.69	0.74	0.77	0.67
Er	1.56	2.59	2.34	1.40	1.81	1.93	1.98	1.75
Tm	0.20	0.35	0.32	0.19	0.26	0.28	0.28	0.26
Yb	1.22	2.18	2.00	1.09	1.72	1.77	1.81	1.50
Lu	0.17	0.31	0.29	0.16	0.25	0.25	0.26	0.23
La_N/Yb_N	37.70	18.39	7.33	38.46	12.25	11.08	11.75	12.23
Eu/Eu*	0.86	0.90	0.93	0.89	0.95	0.92	0.96	0.94
Sample	SZ07-27	SZ07-28	SZ07-30	SZ07-31	JN07-37	JN07-39	JN07-40	JN07-42
Rock type:	D	H.D	D	D	D	D	D	D
Longitude E):	111°51.713′				111°27.547′			
Latitude (N):	41°21.802′				41°28.748′			
SiO_2	46.82	50.79	49.09	52.11	51.99	52.39	52.05	52.83
TiO_2	1.70	1.08	1.32	1.10	0.81	1.21	1.15	0.67
Al_2O_3	18.51	11.13	16.46	10.59	17.00	16.31	17.04	13.47
Fe_2O_3*	11.47	10.10	9.32	10.09	7.61	8.23	8.29	8.59

Sample	SZ07-27	SZ07-28	SZ07-30	SZ07-31	JN07-37	JN07-39	JN07-40	JN07-42
Rock type:	D	H.D	D	D	D	D	D	D
MnO	0.11	0.13	0.10	0.14	0.12	0.10	0.11	0.15
MgO	4.55	11.37	7.49	11.38	6.29	5.88	5.65	9.04
CaO	7.56	9.39	8.82	9.09	7.91	8.09	7.75	9.29
Na_2O	3.60	2.26	2.81	1.99	3.62	3.33	3.36	3.16
K_2O	2.03	1.11	1.85	1.37	2.02	1.89	2.07	1.35
P_2O_5	0.79	0.15	0.28	0.14	0.29	0.18	0.14	0.14
LOI	2.30	1.98	1.92	1.45	1.81	1.92	1.97	1.16
Total	99.44	99.48	99.46	99.45	99.46	99.53	99.58	99.86
Mg-no.	44.0	69.0	61.4	69.1	62.1	58.6	57.4	67.6
Sc	12.1	48.0	29.9	49.5	23.2	28.9	26.8	33.7
V	198	236	215	242	156	235	236	166
Cr	2.49	137	63.9	138	122	119	88.2	323
Co	26.8	46.8	40.4	49.5	29.9	29.4	29.9	40.4
Ni	25.5	86.4	68.0	96.4	66.1	47.8	47.0	106
Ga	23.0	15.6	20.6	15.3	18.3	18.6	19.0	14.5
Rb	34.6	30.7	46.5	37.9	64.9	62.1	62.7	32.6
Sr	1215	558	1036	436	846	837	736	541
Y	20.5	18.22	17.2	18.5	18.8	21.6	19.6	15.7
Zr	85.1	158	124	134	150	112	92.9	124
Nb	8.34	5.86	3.84	6.36	7.98	6.93	7.95	5.17
Cs	1.11	0.42	1.33	0.70	1.35	1.47	1.61	0.50
Ba	784	337	533	301	595	561	547	416
Hf	2.40	4.14	3.39	3.72	3.93	3.30	2.97	3.49
Ta	0.42	0.31	0.24	0.40	0.54	0.37	0.61	0.32
Pb	7.60	7.27	6.57	5.91	12.7	13.1	14.01	10.9
Th	2.84	3.96	1.86	3.95	6.70	6.70	12.24	5.42
U	0.64	0.62	0.46	0.81	1.82	1.65	2.80	2.44
La	28.9	20.9	18.4	22.9	23.1	27.9	28.5	18.6
Ce	66.0	41.5	41.8	45.3	49.6	54.0	53.3	34.5
Pr	9.44	5.02	5.59	5.48	6.78	6.64	6.17	4.68
Nd	37.7	20.5	22.9	21.5	25.9	26.6	24.0	17.6
Sm	8.20	4.70	5.22	4.63	5.67	5.76	5.23	3.70
Eu	2.45	1.30	1.54	1.34	1.53	1.60	1.51	1.04
Gd	6.84	4.38	4.53	4.45	4.61	5.27	4.61	3.33
Tb	0.96	0.67	0.67	0.67	0.71	0.81	0.72	0.52
Dy	4.95	3.70	3.64	3.76	3.93	4.70	4.09	3.02
Ho	0.89	0.73	0.73	0.72	0.80	0.94	0.84	0.61
Er	2.18	1.89	1.87	1.96	2.08	2.39	2.19	1.68
Tm	0.29	0.27	0.26	0.28	0.31	0.35	0.32	0.26
Yb	1.71	1.70	1.53	1.66	2.00	2.16	2.05	1.65
Lu	0.24	0.24	0.23	0.25	0.30	0.32	0.31	0.25
La_N/Yb_N	12.15	8.82	8.61	9.90	8.31	9.24	9.97	8.07
Eu/Eu*	1.00	0.87	0.97	0.91	0.92	0.88	0.94	0.90

*Mg-number = 100 × molar Mg/(Mg + Fe); ($FeO_t = 0.9 \times Fe_2O_3^*$). H.D, hornblende diorite; D, diorite; M.D, monzodiorite.

Such petrological and mafic geochemical characters (low silica contents, high MgO, Cr and Ni) are distinct from those of any crustal materials (Rudnick & Gao 2003) or crustally derived meltsñ (e.g. Patiño Douce & Beard 1995; Patiño Douce & McCarthy 1997), thus arguing strongly for a mantle derivation. This is consistent with enriched mantle parentage generally envisaged for typical appinitic rocks (Bowes & Košler 1993; Fowler & Henney 1996; Fowler *et al*. 2001, 2008; Ye *et al*. 2008) and various sanukitoid suites (Kovalenko *et al*. 2005; Heilimo *et al*. 2010). However, the moderate Mg-numbers and low transitional metal abundances in some samples indicate that they may have experienced some crystal fractionation, most probably of plagioclase, amphibole, biotite, titanite and apatite, as reflected by systematic variations of major oxides and compatible trace elements with MgO and the Cr–Ni fractionation vectors (Fig. 4).

In general, the geochemical signatures of appinitic and sanukitic affinity in the Siziwangqi rocks can be attributed to: (1) hydrous melting of mantle peridotites as a result of the addition of aqueous fluids from slab dehydration (e.g. Hirose 1997); (2) partial melting of subducting lithosphere and interaction of the resultant silicic melts with overlying mantle peridotites (Kelemen 1995); (3) melting of subducting sediments and subsequent melt–mantle interaction (Shimoda *et al*. 1998; Tatsumi 2006); (4) crustal influence during magma ascent (Castro *et al*. 2003; Qian & Hermann 2010; Rapp *et al*. 2010).

Given their cratonic occurrence, the Siziwangqi rocks could have been produced by the assimilation models that applied to

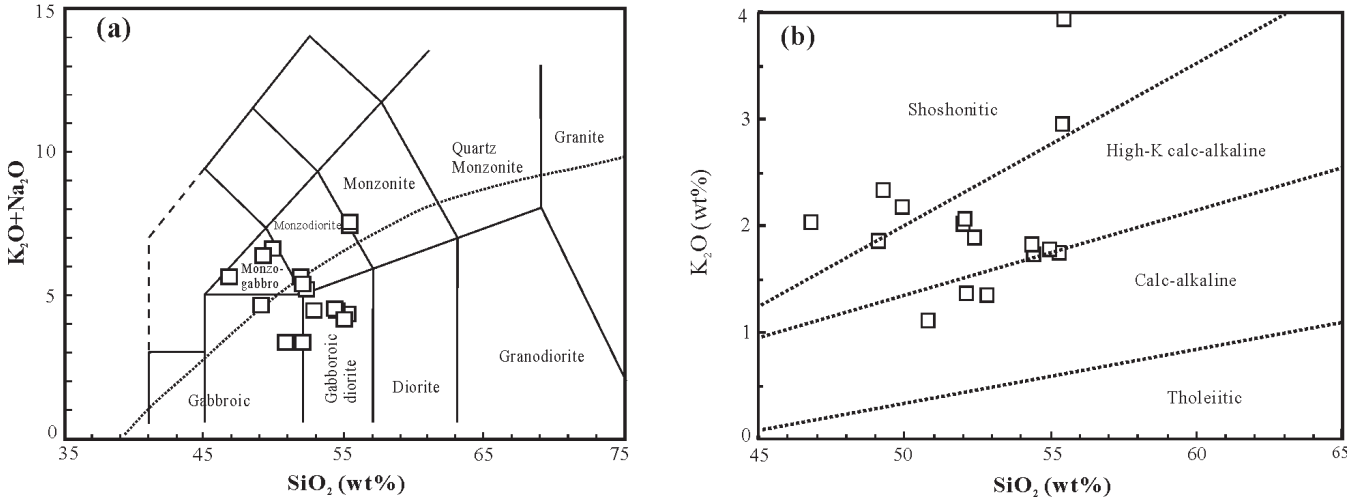

Fig. 3. (**a**) Classification plot of total alkalis v. silica for the appinitic intrusions from southern Inner Mongolia (Le Maitre 2002). The alkaline–tholeiitic division (dotted line) is from Irvine & Baragar (1971). (**b**) SiO_2–K_2O variation plot.

other cratonic sanukitoids. However, they lack any petrographic characters indicative of magma mixing at crustal levels as in the case of the Hanxin high-Mg diorites from the North China craton (Qian & Hermann 2010). In terms of trace elements, the present rocks have much higher Sr abundance (436–1343 ppm) than that of continental crust in general (Rudnick & Gao 2003) and local upper crust country rocks (25–140 ppm) as represented by the khondalites of Zhaertai and Bayan Obo groups (Li *et al*. 2007; Peng *et al*. 2010). Furthermore, they show Sr and Nd isotopic compositions distinct from those of the Archaean TTG gneiss-like lower crust component of the North China craton ($^{87}Sr/^{86}Sr_i$ = 0.710–0.730, $\varepsilon_{Nd}(t)$ = −25 to −43) (Jahn *et al*. 1987, 1999). This argues against such potential basement or country rock assimilants as the source of enrichments observed in the Siziwangqi rocks. However, the Archaean mafic lower crustal component of the craton may have played a role, considering that it directly hosts the Siziwangqi rocks and the data for the rocks also point toward the field for it (Fig. 6). Such contamination would result in negatively correlated $^{87}Sr/^{86}Sr_i$ and Mg-number, or positively correlated $\varepsilon_{Nd}(t)$ and Mg-number. This is not the case for our rocks (Fig. 9), thus disfavouring this potential assimilation. More specifically, those samples (SZ07-28 and SZ07-31) with the lowest $\varepsilon_{Nd}(t)$ are also the most magnesian. This is the opposite of what could be expected during assimilation and fractionation processes within the crust.

These petrogenetic scenarios can be more quantitatively tested by a simple mixing model (Lugmair & Marti 1978) and an assimilation–fractional crystallization (AFC) model (DePaolo 1981) based on the Sr and Nd isotopes of potential end-members, given that conceivable lithospheric mantle end-member can be represented by the Ordovician kimberlites (Yang *et al*. 2009) and some Devonian primitive mafic–ultramafic rocks (Zhang *et al*. 2009*a*). On one hand, simple mixing calculations show that the assimilation of >50% lower crust component into mantle-derived magma is required to match the observed Sr and Nd isotopic compositions of the present rocks (Fig. 6). Such a proportional crustal contribution cannot be reconciled with the mafic composition of the Siziwangqi rocks. On the other hand, an AFC process would result in intermediate to felsic alkaline magmas like the middle Devonian Sandaogou alkaline complex from the same region (Fig. 6; Zhang *et al*. 2010*a*).

Given the arguments above, the Siziwangqi rocks seem to maintain a relatively primary affinity from a subduction-related enriched mantle parentage. Specifically, those samples with high Mg-number (>65) and Cr (150–242 ppm) abundances are most likely to have a composition closest to parental basaltic melts in terms of elemental and isotopic compositions. Accordingly, variable Nd isotopic compositions in these samples attest to a highly heterogeneous enriched mantle source, which may have been formed through some subduction-related metasomatic events.

As is implied in various petrogenetic models for appinitic and sanukitic magmas, the metasomatic agents of subduction affinity can be slab-derived fluids (e.g. Hirose 1997), melts from basaltic oceanic crust (Kelemen 1995) or sediment-derived silicic melts (Fowler *et al*. 2001, 2008; Tatsumi 2006), with each yielding distinctive trace element and isotopic imprint in the metasomatized mantle. Hence their nature can be fingerprinted by ratios between particular elements. For instance, the plot of Ba/La v. Th/Ta is good at discriminating hydrous fluids and melts (McCulloch & Gamble 1991), whereas Ba/Th v. La/Sm can distinguish sediment-related melts from oceanic crust-derived ones. In our case, both plots highlight a dominant contribution from sediment-derived melts (Fig. 10). Low ratios of Rb/Cs (8–73), Ce/Pb (3.2–9.0) and U/Pb (0.06–0.30) in the present rocks are also similar to those of modern oceanic sediments (e.g. Plank & Langmuir 1998). Equally revealing is the elevated $^{87}Sr/^{86}Sr_i$ ratios of 0.7058–0.7093 in the rocks, a well-documented hallmark for subducted sediments (Plank & Langmuir 1998; Patino *et al*. 2000). This closely resembles the sanukitoids of the Setouchi volcanic belt (Japanese arc), whose mantle source was fertilized by subducted sediment-derived melts (Shimoda *et al*. 1998; Tatsumi 2006).

Further complexity arises from the fact that the subducted sediments could include components as diverse as terrigenous sediments, pelagic clays and chemical precipitates (Fe–Mn crusts) (e.g. Plank & Langmuir 1998; Marini *et al*. 2005). These components tend to exhibit distinct REE and HFSE signatures corresponding to their different behaviour during sedimentary processes (Altherr *et al*. 2004; Marini *et al*. 2005). Terrigenous sediments thus have higher ratios of Hf/Sm and Hf/Nd and lower Lu/Hf ratio than pelagic clays and chemical precipitates. The concomitant isotopic variation is a nonradiogenic signature for the former and more radiogenic one for the latter. In our case, the relatively high Hf/Sm (0.44–0.94) and low Nd/Hf (5–16) ratios in the Siziwangqi rocks point to the involvement of a terrigenous component with detrital zircon. On the other hand, the high Ba/Th and Ba/La in

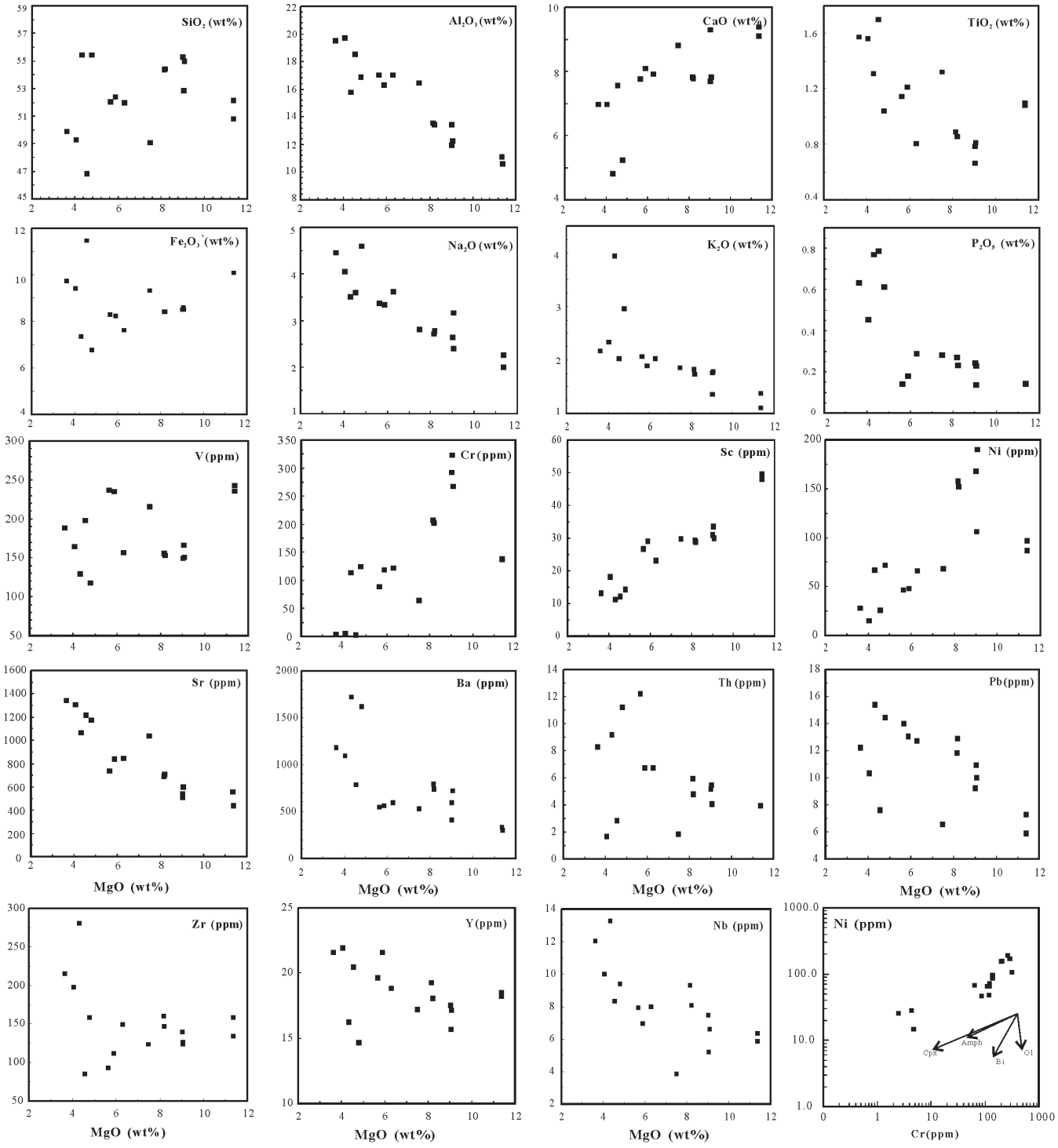

Fig. 4. Plots of major oxides and selected trace elements v. MgO, and plot of Ni v. Cr for the appinitic intrusions from southern Inner Mongolia.

some samples could be due to certain amounts of such Ba-enriched sedimentary component as pelagic clays, whereas the high Sr/Nd ratios (17–45) suggest a significant contribution of carbonate components in the subducted sediment. Therefore, the observed elemental variation, coupled with variable but consistent unradiogenic Nd and Hf isotopic signature, can be explained by the addition of somewhat heterogeneous terrigenous–hemipelagic components to the mantle sources of the Siziwangqi appinitic magmas.

Timing of metasomatism and geodynamic setting

For the protracted evolution of the northern North China craton as a convergent plate margin during Palaeozoic time, various palaeotectonic reconstructions suggest that the Early Palaeozoic orogenic cycle developed through interaction of the oceanic lithosphere that contained the North China block (and South China and other micro-continents) with active margins rimming East

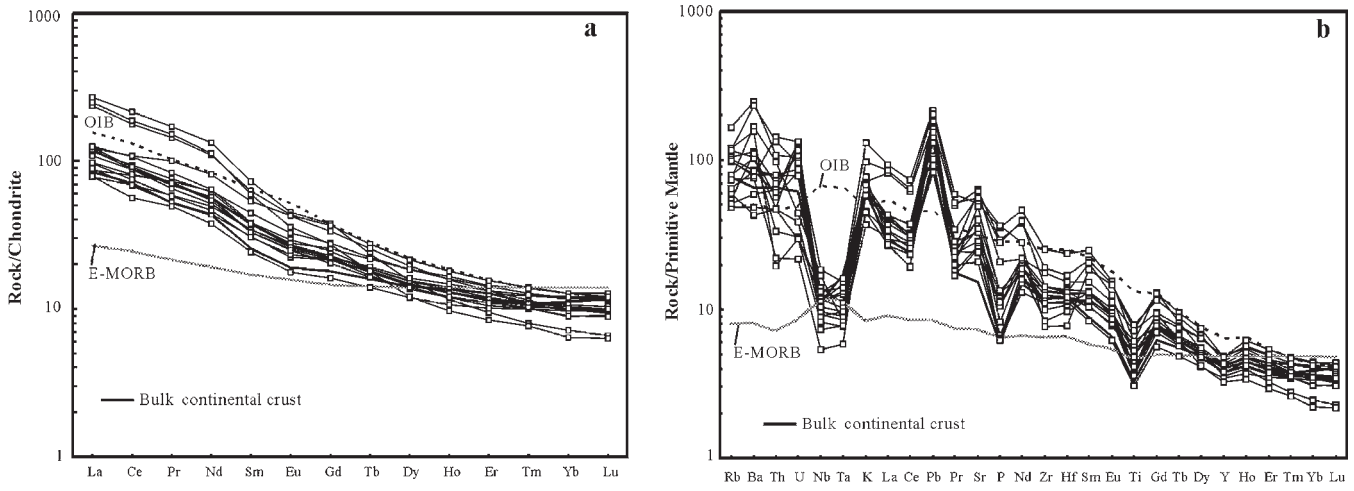

Fig. 5. (**a**) Chondrite-normalized REE patterns and (**b**) primitive mantle-normalized trace element spidergrams for the sanukitic intrusions from southern Inner Mongolia. Normalization values are from Sun & McDonough (1989). The data for oceanic island basalt (OIB) and enriched mid-ocean ridge basalt (E-MORB) are also from Sun & McDonough (1989). Bulk continental crust data are from Rudnick & Gao (2003).

Table 2. *Rb–Sr and Sm–Nd isotopic compositions for the appinitic intrusions from south Inner Mongolia*

Sample no.	Rb (ppm)	Sr (ppm)	$^{87}Rb/^{86}Sr$	$^{87}Sr/^{86}Sr$	±2σ	$(^{87}Sr/^{86}Sr)_t$	Sm	Nd	$^{147}Sm/^{144}Nd$	$^{143}Nd/^{144}Nd$	±2σ	Initial Nd	$\varepsilon_{Nd}(t)$	T_{DM} (Ma)	T_{DM2} (Ma)
SZ07-11	136.0	1108	0.3552	0.707986	0.000012	0.70637	10.775	64.99	0.1002	0.511979	0.000014	0.511769	−8.92	1266	1569
SZ07-15	51.83	1343	0.1117	0.707761	0.000013	0.70725	8.377	48.14	0.1052	0.511746	0.000013	0.511526	−13.68	1966	2186
SZ07-25	64.75	725.3	0.2584	0.708272	0.000012	0.70710	5.460	29.07	0.1135	0.511954	0.000021	0.511716	−9.95	1814	1884
SZ07-26	47.87	632.5	0.2191	0.708178	0.000012	0.70718	5.021	25.85	0.1174	0.511844	0.000012	0.511598	−12.26	2060	2070
SZ07-28	29.90	601.8	0.1439	0.709650	0.000013	0.7090	4.677	21.13	0.1338	0.511834	0.000011	0.511554	−13.13	2498	2137
SZ07-30	41.80	1115	0.1085	0.706283	0.000011	0.70579	5.089	24.31	0.1266	0.511936	0.000015	0.511671	−10.84	2116	1954
SZ07-31	20.21	506.0	0.1156	0.709802	0.000016	0.70928	5.559	25.58	0.1314	0.511815	0.000014	0.511540	−13.40	2459	2158
JN07-37	7.878	909.3	0.0251	0.708317	0.000012	0.70820	4.482	22.91	0.1183	0.511932	0.000014	0.511714	−10.58	1940	1934
JN07-39	43.21	892.0	0.1402	0.708478	0.000010	0.70784	5.508	25.83	0.1289	0.511961	0.000012	0.511691	−10.45	2129	1922
JN07-40	6.161	825.5	0.0216	0.708552	0.000010	0.70845	5.710	26.93	0.1282	0.511932	0.000013	0.511663	−10.99	2163	1965

$^{87}Sr/^{86}Sr_i = (^{87}Sr/^{86}Sr)_{sample} - (^{87}Rb/^{86}Sr)_{sample} \times (e\lambda^t - 1)$, $\lambda = 1.42 \times 10^{-11}\ a^{-1}$ (Steiger & Jäger 1977); initial $Nd = (^{143}Nd/^{144}Nd)_{sample} - (^{147}Sm/^{144}Nd)_{sample} \times (e\lambda^t - 1)$, $\varepsilon_{Nd} = ((^{143}Nd/^{144}Nd)_{sample}/(^{143}Nd/^{144}Nd)_{CHUR} - 1) \times 10\,000$, $f_{Sm/Nd} = (^{147}Sm/^{144}Sm)_{sample}/(^{147}Sm/^{144}Sm)_{CHUR} - 1$, $T_{DM} = 1/\lambda \times \ln(1 + ((^{143}Nd/^{144}Nd)_{sample} - 0.51315)/((^{147}Sm/^{144}Nd)_{sample} - 0.2137)$, where $(^{147}Sm/^{144}Nd)_{CHUR} = 0.1967$, $(^{143}Nd/^{144}Nd)_{CHUR} = 0.512638$, $\lambda_{SM} = 6.54 \times 10^{-12}\ a^{-1}$ (Lugmair & Marti 1978).

Gondwana (Li & Powell 2001; Veevers 2004; de Jong *et al*. 2006). The post-collisional magmatic suite along the northern North China craton, such as Early to Middle Devonian alkaline rocks (Zhang *et al*. 2010*a*) and mafic–ultramafic complexes (Zhang *et al*. 2009*b*), marked its termination. Specifically, we ascribed this episode of magmatism to a tectonic regime of slab breakoff (Zhang *et al*. 2010*a*).

After the Early Devonian, the North and South China cratons began to separate from the Cimmerian margin of Gondwana and initiated a northward drift (Li & Powell 2001; de Jong *et al*. 2006). Subduction resumed when this drift led to collision with the Angaran active margin of Siberia by means of subduction of the Palaeo-Asian Ocean (de Jong *et al*. 2006). Although a Late Palaeozoic northward subduction system is manifest by a series of Devonian to Carboniferous arc magmatic rocks and Early Permian post-collisional alkaline magmatic rocks from the terranes in south Mongolia (Blight *et al*. 2010*a*, *b*) and the northern China block (Chen *et al*. 2000; Zhang *et al*. 2008, 2011*b*; Jian *et al*. 2010), the geodynamic setting along the side of the North China craton remains controversial. The current prevailing model is that an Andean-style continental arc developed there as a result of the southward subduction in the Solonker suture zone (Zhang *et al*. 2007, 2009*a*, *b*), with which we previously concurred (Zhang & Zhai 2010).

These seemingly discrete Phanerozoic subduction events, together with the recently documented Palaeoproterozoic ridge-subduction event (Peng *et al*. 2010), imply that multiple subduction-related metasomatic events may have occurred in the region. It is not easy to discriminate these events. However, it is likely that that the metasomatism is related to the subduction process that finally led to the Devonian amalgamation between the North China craton and the Bainaimiao arc terrane (Zhang *et al*. 2010*a*), given the comparable unradiogenic isotopic values in the Siziwangqi rocks and modern oceanic sediments (Plank & Langmuir 1998; Marini *et al*. 2005), and the following argument against an active continental arc model for the northern North China craton during late Palaeozoic time.

Admittedly, the Andean-style active continental arc model is an expedient choice for explaining the magmatic activities along ancient convergent plate margins. However, its application to the Carboniferous situation in the northern North China craton presents serious challenges. First, it seems to contradict the recent proposition that the southward subduction in the Solonker zone did not initiate until *c*. 294–280 Ma (Jian *et al*. 2010). Second, the sparsely

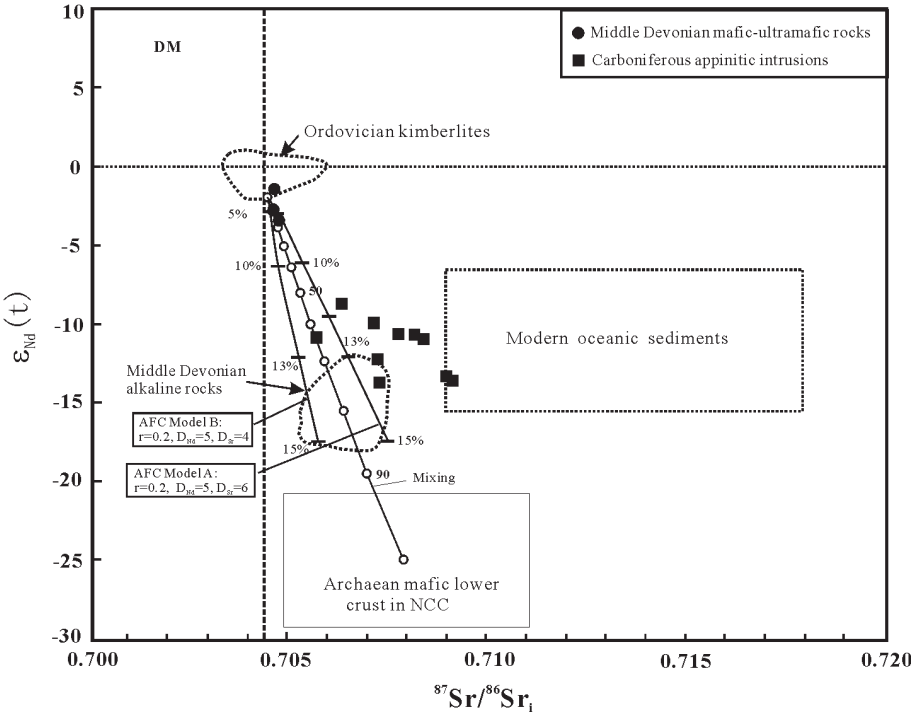

Fig. 6. Plot of initial $\varepsilon_{Nd}(t)$ v. $^{87}Sr/^{86}Sr_i$ for the appinitic intrusions from southern Inner Mongolia. The fields for the Ordovician kimberlites and the middle Devonian alkaline complex from the North China craton are from Yang *et al*. (2009) and Zhang *et al*. (2010*a*). The data for the middle Devonian mafic–ultramafic rocks are from Zhang *et al*. (2009*b*). Archaean mafic lower crust of the North China craton is from Jahn *et al*. (1987, 1999). The mixing and AFC modelling parameters used for lower crust-derived melts of the North China craton are Sr = 300 ppm, $^{87}Sr/^{86}Sr = 0.708$, Nd = 25 ppm and $\varepsilon_{Nd} = -25$, and for lithospheric mantle derived melts are Sr = 1000 ppm, $^{87}Sr/^{86}Sr = 0.7045$, Nd = 70 ppm and $\varepsilon_{Nd} = -2$. The field for the modern oceanic sediments is from Plank & Langmuir (1998) and Patino *et al*. (2000).

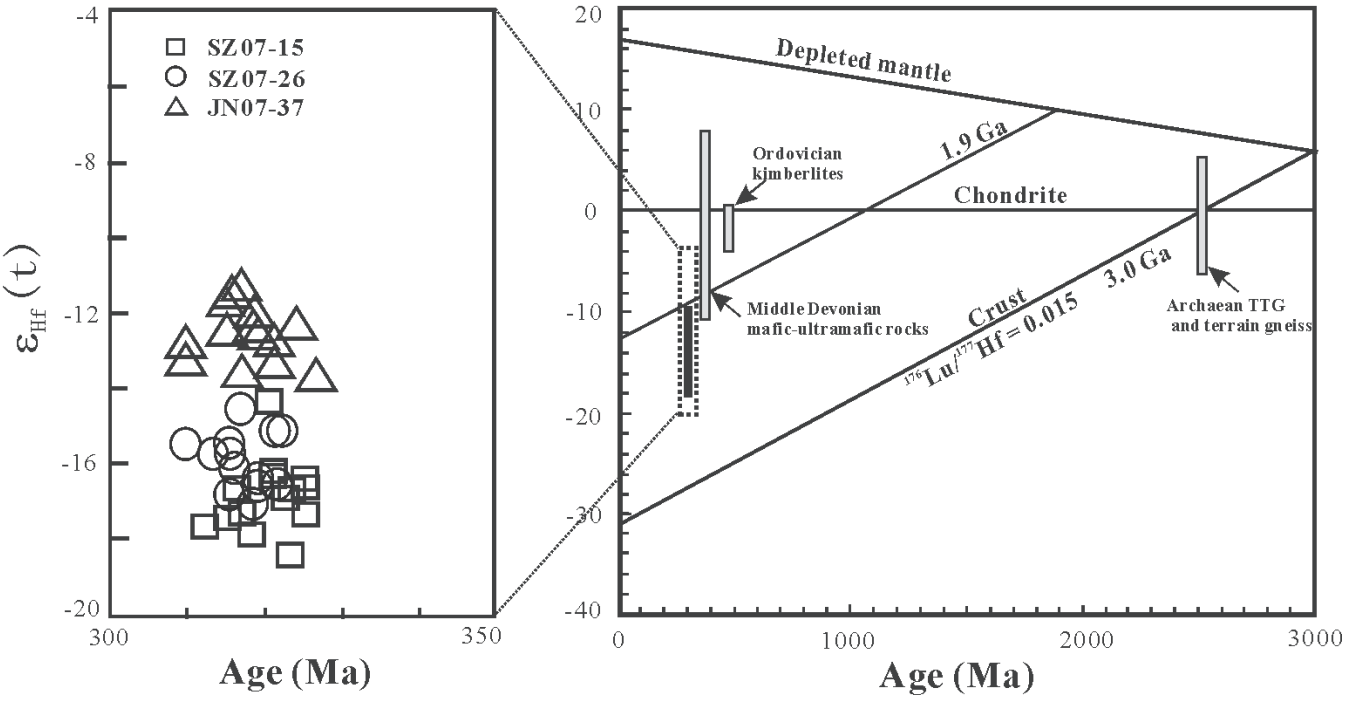

Fig. 7. $\varepsilon_{Hf}(t)$ v. U–Pb age plot for zircons from the appinitic intrusions from southern Inner Mongolia. The fields for the Ordovician kimberlites, the middle Devonian mafic–ultramafic rocks, and the Archaean TTG and terrane gneiss from the northern North China craton are from Yang *et al*. (2009), Zhang *et al*. (2009*a*) and Yang *et al*. (2008), respectively.

scattered Carboniferous plutons along the northern North China craton contrast sharply with the large-scale active continental arc magmatism that generally constitutes a significant fraction of an active continental margin, as typified by the Mesozoic Cordilleran batholiths (Ducea 2001; Wenner & Coleman 2004) and the Mesozoic to Cenozoic magmatic rocks from the Central Andes (e.g. Lucassen *et al*. 2006; Mamani *et al*. 2010). Third, although several Andean examples illustrate some contribution of ancient crust materials to active continental arc magmatism, significant enrichment is observed only in more restricted geological time and coincident with crustal thickening (Ducea & Barton 2007; Mamani *et al*. 2010; Collins *et al*. 2011). The contribution from subarc

depleted mantle sources and resultant significant crustal growth remain a central theme during the long history of the Andean continental arc evolution. This is not the case in the late Palaeozoic northern North China craton. This study and previous investigations on the Early Devonian to Early Permian magmatic rocks from this region consistently document predominant magma sources of subcontinental lithospheric mantle and lower crust (Zhang *et al*. 2007, 2009*a*, *b*, 2010*a*, 2011*a*; Chen *et al*. 2009). This implies that only slight amounts of juvenile materials, if any, have been added during this period.

Not coincidently, such a reworking-dominated crustal evolutionary scenario is compatible with the two contrasting Phanerozoic orogenic systems recorded by zircon hafnium isotope data from orogens worldwide since 550 Ma ago (Collins *et al*. 2011). As represented by the North American case, the symmetrical, external (circum-Pacific) system features a contracting Hf isotopic array towards more radiogenic signature, reflecting semi-continuous subduction of oceanic lithosphere beneath continental lithosphere and concomitant protracted addition of juvenile crust to the orogenic segments (Bahlburg 2011; Collins *et al*. 2011). By contrast, the asymmetrical, internal orogenic system, with the Central Asian Orogenic Belt as one essential component, displays a fanning Hf isotopic array, testifying to the long-term subduction that led to fragmentation and collision of ancient continents or continental fragments (Collins *et al*. 2011). Superimposed on this predominantly north-directed subduction scenario is short-term, localized south-dipping subduction possibly triggered by intermittent slab flipping during closure of back-arc basins or subduction ribbons (Collins *et al*. 2011), as is exemplified by the specific case of flipping from north to south in the Solonker suture zone during Early Permian time (Zhang *et al*. 2011*b*).

Noting its dual cratonic and reactivated characters, we suggest that the late Palaeozoic situation in the northern North China craton can be likened to a metacratonic evolution (Zhang *et al*. 2011*a*). As exemplified by the Saharan metacraton, a metacraton evolves from a region between a rigid, unaffected craton and a mobile belt completely affected by an orogeny (Abdelsalam *et al*. 2002; Liégeois *et al*. 2003). It has been remobilized during an orogenic event but is still recognizable through its rheological, petrological, geochronological and isotopic characteristics (Liégeois *et al*. 2003; De Waele *et al*. 2006). In general, a metacratonic evolution can be driven by a succession of events including collisional process, linear lithospheric delamination along mega-shear zones, regional extension and post-collisional dismembering (Abdelsalam *et al*. 2002; Liégeois *et al*. 2003). These processes are conducive to episodic magmatism with long-term memory of cratonic geochemical signature, recurrent transcurrent movements along pre-existing lithospheric shear zones, coexisting low- and high-grade metamorphism, and favourable fluid circulation (Abdelsalam *et al*. 2002; Liégeois *et al*. 2003; De Waele *et al*. 2006; Ennih & Liégeois 2008).

More specifically, numerous case studies have documented a viable regime of post-subduction slab breakoff for triggering mantle melting to form appinitic and sanukitic magmas (Atherton & Ghani 2002; Kovalenko *et al*. 2005; Lobach-Zhuchenko *et al*. 2005; Ye *et al*. 2007; Heilimo *et al*. 2010). In our case, the present rocks, plus other previously documented coeval hornblende-rich mafic complexes and adakitic granites from neighbouring regions (Zhang *et al*. 2007, 2009*a*, *b*), are reminiscent of the high Ba–Sr appinite–granite suite from the British Caledonides (Fowler & Henney 1996; Fowler *et al*. 2001, 2008; Atherton & Ghani 2002) and the Tibet Plateau (Ye *et al*. 2008). Such a characteristic magmatic association has been invariably attributed to post-orogenic slab breakoff (Atherton & Ghani 2002) or slab delamination

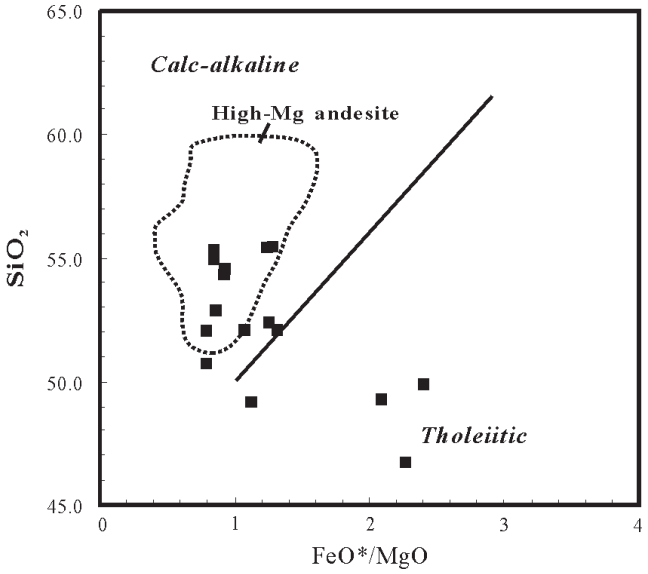

Fig. 8. Plot of SiO_2 v. FeO*/MgO. The field for high-Mg andesites is from Kamei *et al*. (2004).

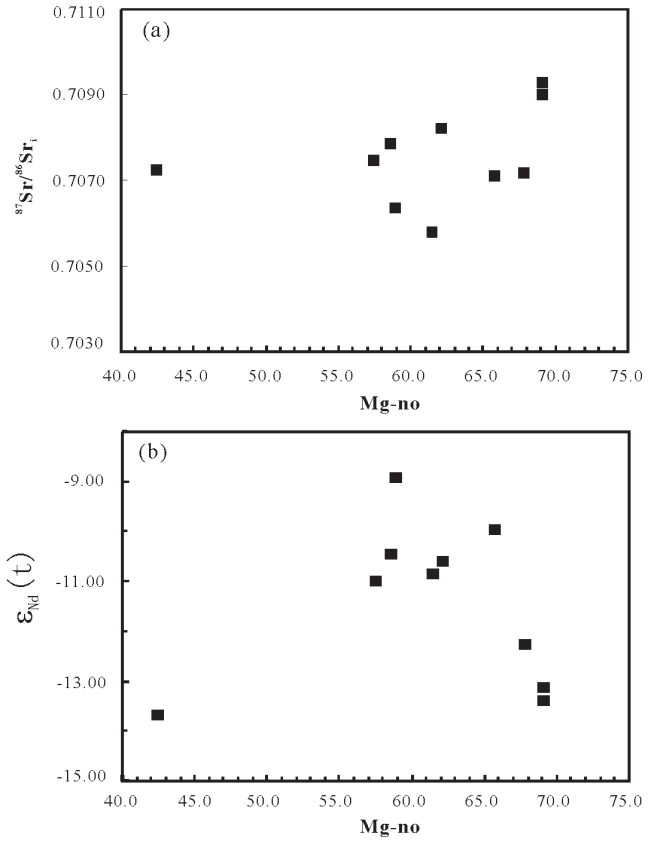

Fig. 9. Plots of (**a**) $^{87}Sr/^{86}Sr_i$ v. Mg-no and (**b**) $\varepsilon_{Nd}(t)$ v. Mg-no.

(Ye *et al*. 2008). Equally remarkable is the occurrence of late Palaeozoic eclogites in the region studied (Ni *et al*. 2006). With their protolith age of *c*. 438 Ma and high-pressure metamorphic age of *c*. 325 Ma (Ni *et al*. 2006), these eclogites may represent the metamorphic products of previously subducted Palaeo-Asian

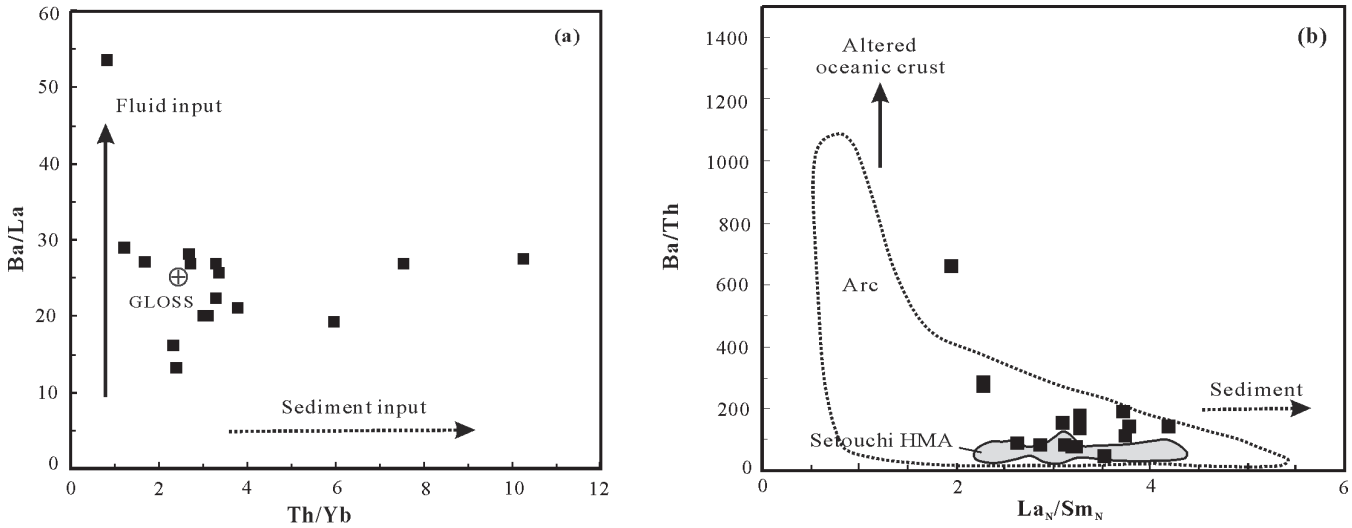

Fig. 10. (**a**) Ba/La v. Th/Yb and (**b**) Ba/Th v. La_N/Sm_N plots for the appinitic intrusions from southern Inner Mongolia. In (**a**), continuous-line vector, slab-derived fluids; dashed-line vector, sediment input in the source as represented and discussed by Woodhead *et al*. (2001). Global subducting sediment (GLOSS) compositions are from Plank & Langmuir (1998). In (**b**), subscript 'N' denotes chondrite-normalized values; the fields for arc and Setouchi high-Mg andesites (HMA) are from Tatsumi (2006).

oceanic crust as a natural consequence of slab breakoff (Davies & von Blanckenburg 1995). Therefore, we suggest that these magmatic and metamorphic expressions may attest to another slab breakoff event, besides the earlier breakoff event as monitored by Devonian alkaline magmatism (Zhang *et al*. 2010*a*).

Like the British Caledonides, the North China craton represents a classic area of Phanerozoic high Ba–Sr granitoid (Qian *et al*. 2003) or potassium-rich adakitic magmatism (Jiang *et al*. 2007). The present appinitic rocks, together with other episodes of late Palaeozoic to Mesozoic amphibole-rich mafic to intermediate intrusions of the craton (Wang *et al*. 2006; Chen *et al*. 2009; Zhang *et al*. 2009*b*; Qian & Hermann 2010), may constitute an extensive newly accreted basaltic underplate within the middle to lower crust of the North China craton. As with its Caledonian counterparts, this enriched underplate should be essential for the formation of voluminous Mesozoic adakitic granites in the North China craton, functioning either as contemporaneous mafic precursor in the case of an AFC model (Qian *et al*. 2003) or as progenitor protolith in the case of a crustal anatexis model (Jiang *et al*. 2007). Clearly, evaluating the merit of either scenario necessitates full characterization of various rock constituents of single batholiths.

Conclusions

LA-ICP-MS zircon U–Pb dating constrains a Carboniferous emplacement age of *c*. 320–317 Ma for a series of mafic to intermediate intrusions from south Inner Mongolia along the northern margin of the North China craton. These rocks exhibit a hornblende-dominated appinitic petrographic character and a sanukitic geochemical affinity. Geochemical and isotopic tracing demonstrates that a distinctive two-stage process contributed to their generation: a precursory metasomatism stage of mantle peridotites by melts from subduction-related sediments, and a lagged partial melting stage probably owing to post-subduction slab breakoff or delamination event. These appinitic intrusions, plus other coeval mafic–ultramafic complex and high Ba–Sr granites from neighbouring regions, not only witness a heterogeneously enriched subcontinental lithospheric mantle along the northern North China craton, but also attest to a metacratonic process within a post-subduction transtensional regime possibly featuring multiple slab breakoff events.

We thank He Li and Xindi Jin for their help in major- and trace-element analysis; Chaofeng Li and Yanbing Zhang for their help in Sr–Nd and zircon Hf isotope analyses; Haihong Chen for her help in LA-ICP-MS zircon U–Pb dating. We are also grateful to M. B. Fowler, Shuanhong Zhang and subject editor M. Cho for their critical comments, which substantially improved the paper. This study is financially supported by the Knowledge Innovation Program of the Chinese Academy of Sciences (Grant Nos. KZCX2-YW-QN115 and KZCX2-YW-Q4-04) and the National Natural Science Foundation of China (Grant Nos. 90914008 and 40873026).

References

Abdelsalam, M., Liégeois, J.P. & Stern, R.J. 2002. The Saharan metacraton. *Journal of African Earth Science*, **34**, 119–136.

Altherr, R., Meyer, H.P., Holl, A., Volker, F., Alibert, C., McCulloch, M.T. & Majer, V. 2004. Geochemical and Sr–Nd–Pb isotopic characteristics of Late Cenozoic leucite lamproites from the East European alpine belt (Macedonia and Yugoslavia). *Contributions to Mineralogy and Petrology*, **147**, 58–73.

Anderson, T. 2002. Corrections of common lead in U–Pb analyses that do not report ^{204}Pb. *Chemical Geology*, **192**, 59–79.

Atherton, M.P. & Ghani, A.A. 2002. Slab breakoff: a model for Caledonian, Late Granite syn-collisional magmatism in the orthotectonic (metamorphic) zone of Scotland and Donegal, Ireland. *Lithos*, **62**, 65–85.

Ayrton, S.N. 1991. Appinites, lamprophyres and mafic magmatic enclaves: three related products of interaction between acid and mafic magmas. *In*: Didier, J. & Barbarin, B. (eds) *Enclaves and Granite Petrology*. Developments in Petrology, **13**, 465–478.

Badarch, G., Cunningham, W.D. & Windley, B.F. 2002. A new terrane subdivision for Mongolia: implications for the Phanerozoic crustal growth of Central Asia. *Journal of Asian Earth Sciences*, **21**, 87–104.

Bahlburg, H. 2011. Mantle-controlled mountains. *Nature Geosciences*, **4**, 280–282.

Bailey, E.B. & Maufe, H.B. 1916. *The Geology of Ben Nevis and Glen Coe and the Surrounding Country*. Memoirs of the Geological Survey of Scotland, 247.

Bea, F., Montero, P. & Molina, J.F. 1999. Mafic precursors, peraluminous granitoids, and lamprophyres in the Avila batholith: a model for the generation of Variscan batholiths in the Iberia. *Journal of Geology*, **107**, 399–419.

BLIGHT, J.H.S., CROWLEY, Q.G., PETTERSON, M.G. & CUNNINGHAM, D. 2010*a*. Granites of the southern Mongolia Carboniferous arc: new geochronological and geochemical constraints. *Lithos*, **116**, 35–52.

BLIGHT, J.H.S., PETTERSON, M.G., CROWLEY, Q.G. & CUNNINGHAM, D. 2010*b*. The Oyut Ulaan volcanic group: stratigraphy, magmatic evolution and timing of Carboniferous arc development in SE Mongolia. *Journal of the Geological Society, London*, **167**, 491–509.

BOWES, D.R. & KOŠLER, J. 1993. Geochemical comparisons of the subvolcanic appinite suites of the British Caledonides and the durbachite suite of the central European Hercynides: evidence for associated shoshonitic and granitic magmatism. *Mineralogy and Petrology*, **48**, 47–63.

CASTRO, A., CORRETGÉ, L.G., DE, LA, ROSA, J.D., FERNANDEZ, C., LÓPEZ, S., GARCÍA-MORENO, O. & CHACÓN, H. 2003. The appinite–migmatite complex of Sanabria, NW Iberian Massif, Spain. *Journal of Petrology*, **44**, 1309–1344.

CHEN, B., JAHN, B.M., WILDE, S. & XU, B. 2000. Two contrasting Paleozoic magmatic belts in northern Inner Mongolia, China: petrogenesis and tectonic implications. *Tectonophysics*, **328**, 157–182.

CHEN, B., SUZUKI, K., TIAN, W., JAHN, B.M. & IRELAND, T. 2009. Geochemistry and Os–Nd–Sr isotopes of the Gaositai Alaskan-type ultramafic complex from the northern North China Craton: implications for mantle–crust interaction. *Contributions to Mineralogy and Petrology*, **158**, 683–702.

COLLINS, W.J., BELOUSOVA, E.A., KEMP, A.I.S. & MURPHY, B. 2011. Two contrasting Phanerozoic orogenic systems revealed by hafnium isotope data. *Nature Geosciences*, **4**, 333–337.

DAVIES, J.H. & VON BLANCKENBURG, F. 1995. Slab breakoff: a model of lithosphere detachment and its test in the magmatism and deformation of collisional orogens. *Earth and Planetary Science Letters*, **129**, 85–102.

DE JONG, K., XIAO, W., WINDLEY, B.F., MASAGO, H. & LO, C.H. 2006. Ordovician ^{40}Ar–^{39}Ar phengite ages from the blueschist-facies Ondor Sum subduction–accretion complex (Inner Mongolia) and implications for the early Paleozoic history of continental blocks in China and adjacent areas. *American Journal of Science*, **306**, 799–845.

DEPAOLO, D.J. 1981. Trace element and isotopic effects of combined wallrock assimilation and fractional crystallization. *Earth and Planetary Science Letters*, **53**, 189–202.

DE WAELE, B., LIÉGEOIS, J.P., NEMCHIN, A.A. & TEMBO, F. 2006. Isotopic and geochemical evidence of Proterozoic episodic crustal reworking within the Irumide belt of south–central Africa, the southern metacratonic boundary of an Archaean Bangweulu Craton. *Precambrian Research*, **148**, 225–256.

DUCEA, M. 2001. The California arc: thick granite batholiths, eclogitic residues, lithospheric-scale thrusting, and magmatic flare-ups. *GSA Today*, **11**, 4–10.

DUCEA, M. & BARTON, M.D. 2007. Igniting flare-up events in Cordilleran arcs. *Geology*, **35**, 1047–1050.

ENNIH, N. & LIÉGEOIS, J.P. 2008. The boundaries of the West African Craton, with special reference to the basement of the Moroccan metacratonic anti-Atlas belt. *In*: ENNIH, N. & LIÉGEOIS, J.P. (eds) *The Boundaries of the West African Craton*. Geological Society, London, Special Publications, **297**, 1–17.

FOWLER, M.B. & HENNEY, P.J. 1996. Mixed Caledonian appinite magmas: implications for lamprophyre fractionation and high Ba–Sr granite genesis. *Contributions to Mineralogy and Petrology*, **126**, 199–215.

FOWLER, M.B., HENNEY, P.J., DARBYSHIRE, D.P.F. & GREENWOOD, P.J. 2001. Petrogenesis of high Ba–Sr granites: the Rogart pluton, Sutherland. *Journal of the Geological Society, London*, **158**, 521–534.

FOWLER, M.B., KOCKS, H., DARBYSHIRE, D.P.F. & GREENWOOD, P.B. 2008. Petrogenesis of high Ba–Sr plutons from the Northern Highlands Terrane of the British Caledonian Province. *Lithos*, **105**, 129–148.

GRIFFIN, W.L., POWELL, W.J., PEARSON, N.J. & O'REILLY, S.Y. 2008. GLITTER: data reduction software for laser ablation ICP-MS. *In*: SYLVESTER, P. (ed.) *Laser Ablation-ICP-MS in the Earth Sciences*. Mineralogical Association of Canada, Short Course Series, **40**, 204–207.

HEILIMO, E., HALLA, J. & HÖLTTÄ, P. 2010. Discrimination and origin of the sanukitoid series: geochemical constraints from the Neoarchean western Karelian Province (Finland). *Lithos*, **115**, 27–39.

HIROSE, K. 1997. Melting experiments on lherzolite KLB-1 under hydrous conditions and generation of high-magnesian andesitic melts. *Geology*, **25**, 42–44.

IMBGMR, 1972. *1:200 000 scale geological map of Siziwanqi and notes*. Inner Mongolian Bureau of Geology and Mineral Resources, Hohhot, Mongolia.

IMBGMR, 1975. 1:200 000 scale geological map of Sandaogou and notes. Inner Mongolian Bureau of Geology and Mineral Resources, Hohhot, Mongolia.

IRVINE, T.N. & BARAGAR, W.R.A. 1971. A guide to the chemical classification of the common volcanic rocks. *Canadian Journal of Earth Sciences*, **8**, 523–548.

JAHN, B.M., AUVRAY, B., CORNICHET, J., BAI, Y.L., SHEN, Q.H. & LIU, D.Y. 1987. 3.5 Ga old amphibolites from eastern Hebei province, China: field occurrence, petrology, Sm–Nd isochron age and REE geochemistry. *Precambrian Research*, **34**, 311–346.

JAHN, B.M., WU, F.Y., LO, C.H. & TSAI, C.H. 1999. Crust–mantle interaction induced by deep subduction of the continental crust: geochemical and Sr–Nd isotopic evidence from post-collisional mafic–ultramafic intrusions of the northern Dabie complex, central China. *Chemical Geology*, **157**, 119–146.

JIAN, P., LIU, D.Y., *ET AL*. 2008. Time scale of an early to mid-Paleozoic orogenic cycle of the long-lived Central Asian orogenic belt, Inner Mongolia of China: implications for continental growth. *Lithos*, **101**, 233–259.

JIAN, P., LIU, D.Y., *ET AL*. 2010. Evolution of a Permian intraoceanic arc–trench system in the Solonker suture zone, Central Asian orogenic belt, China and Mongolia. *Lithos*, **118**, 169–190.

JIANG, N., LIU, Y.S., ZHOU, W.G., YANG, J.H. & ZHANG, S.Q. 2007. Derivation of Mesozoic adakitic magmas from ancient lower crust in the North China Craton. *Geochimica et Cosmochimica Acta*, **71**, 2591–2608.

KAMEI, A., OWADA, M., NAGAO, T. & SHIRAKI, K. 2004. High-Mg diorites derived from sanukitic HMA magmas, Kyushu Island, southwest Japan arc: evidence from clinopyroxene and whole rock compositions. *Lithos*, **75**, 359–371.

KELEMEN, P.B. 1995. Genesis of high Mg# andesites and the continental crust. *Contributions to Mineralogy and Petrology*, **120**, 1–19.

KOVALENKO, A., CLEMENS, J.D. & SAVATENKOV, V. 2005. Petrogenetic constraints for the genesis of Archaean sanukitoid suites: geochemistry and isotopic evidence from Karelia, Baltic Shield. *Lithos*, **79**, 147–160.

KUSKY, T.M., WINDLEY, B.F. & ZHAI, M.G. 2007. Tectonic evolution of the North China Block: from orogen to craton to orogen. *In*: ZHAI, M.G., WINDLEY, B.F., KUSKY, T.M. & MENG, Q.R. (eds) *Mesozoic Sub-Continental Lithospheric Thinning Under Eastern Asia*. Geological Society, London, Special Publications, **280**, 1–34.

LEAKE, B.E., WOOLLEY, A.R. *ET AL*. 1997. Nomenclature of amphiboles: report of the subcommittee on amphiboles of the International Mineralogical Association, Commission on New Minerals and Mineral Names. *American Mineralogist*, **82**, 1019–1037.

LE MAITRE, R.W. 2002. *A Classification of Igneous Rocks and a Glossary of Terms: Recommendations of the International Union of Geological Sciences Sub-Commission on the Systematics of Igneous Rocks*. Blackwell, Oxford.

LI, Q.L., CHEN, F.K., GUO, J.H., LI, X.H., YANG, Y.H. & SIEBEL, W. 2007. Zircon ages and Nd–Hf isotopic composition of the Zhaertao Group (Inner Mongolia): evidence for early Proterozoic evolution of the northern North China Craton. *Journal of Asian Earth Sciences*, **30**, 573–590.

LI, Z.X. & POWELL, C.M. 2001. An outline of the paleogeographic evolution of the Australasia region since the beginning of the Neoproterozoic. *Earth-Science Reviews*, **53**, 237–277.

LIÉGEOIS, J.P., LATOUCHE, L., BOUGHRARA, M., NAVEZ, J. & GUIRAUD, M. 2003. The LATEA metacraton (central Hoggar, Tuareg shield, Algeria): behaviour of an old passive margin during the Pan-African orogeny. *Journal of African Earth Sciences*, **37**, 161–190.

LIU, Y., GAO, S., HU, Z., GAO, C., ZONG, K. & WANG, D. 2010. Continental and oceanic crust recycling-induced melt peridotite interactions in the Trans-North China orogen: U–Pb dating, Hf isotopes and trace elements in zircons of mantle xenoliths. *Journal of Petrology*, **51**, 537–571.

LOBACH-ZHUCHENKO, S.B., ROLLINSON, H., *ET AL*. 2005. The Archaean sanukitoid series of the Baltic Shield: geological setting, geochemical characteristics and implications for their origin. *Lithos*, **79**, 107–128.

LUCASSEN, F., KRAMER, W., BARTSH, V., WIKE, H.G., FRANZ, G., ROMER, R.L. & DULSKI, P. 2006. Nd, Pb, and Sr isotope composition of juvenile magmatism in the Mesozoic large magmatic province of northern Chile (18–27°S): indications for a uniform subarc mantle. *Contributions to Mineralogy and Petrology*, **152**, 571–589.

LUDWIG, K. 2001. *User Manual for Isoplot/EX (2.49)*. Berkeley Geochronology Center Special Publication, **1a**.

LUGMAIR, G.W. & MARTI, K. 1978. Lunar initial $^{143}Nd/^{144}Nd$: differential evolution of the lunar crust and mantle. *Earth and Planetary Science Letters*, **39**, 349–357.

MA, L.F. 2002. *Geological Atlas of People's Republic of China*. Chinese Map Publishing House, Beijing.

MAMANI, M., WORNER, G. & SEMPERE, T. 2010. Geochemical variations in igneous rocks of the Central Andean orocline (13°S to 18°S): tracing crustal thickening and magma generation through time and space. *Geological Society of America Bulletin*, **122**, 162–182.

MARINI, J.C., CHAUVEL, C. & MAURY, R.C. 2005. Hf isotope compositions of northern Luzon arc lavas suggest involvement of pelagic sediments in their source. *Contributions to Mineralogy and Petrology*, **149**, 216–232.

MCCULLOCH, M.T. & GAMBLE, J.A. 1991. Geochemical and geodynamical constraints on subduction zone magmatism. *Earth and Planetary Science Letters*, **102**, 358–374.

NI, Z.Y., ZHAI, M.G., WANG, R.M. & TONG, Y. 2006. Late Paleozoic retrograded eclogites from within the northern margin of the North China Craton: evidence for subduction of the Paleo-Asian ocean. *Gondwana Research*, **9**, 209–224.

Patiño Douce, A.E. & Beard, J.S. 1995. Dehydration-melting of biotite gneiss and quartz amphibolite from 3 to 15 kbar. *Journal of Petrology*, **36**, 707–738.

Patiño Douce, A.E. & McCarthy, T.C. 1997. Melting of crustal rocks during continental collision and subduction. *In*: Hacker, B.R. & Liou, J.G. (eds) *When Continents Collide: Geodynamics and Geochemistry of Ultrahigh-Pressure Rocks*. Kluwer, Dordrecht, 27–55.

Patino, L.C., Carr, M.J. & Feigenson, M.D. 2000. Local and regional variations in Central American arc lavas controlled by variations in subducted sediment input. *Contributions to Mineralogy and Petrology*, **138**, 265–283.

Peng, P., Guo, J.H., Zhai, M.G. & Bleeker, W. 2010. Paleoproterozoic gabbronoritic and granitic magmatism in the northern margin of the North China Craton: evidence of crust–mantle interaction. *Precambrian Research*, **183**, 635–659.

Pitcher, W.S. 1997. *The Nature and Origin of Granite*. Chapman & Hall, Glasgow.

Plank, T. & Langmuir, C. 1998. The chemical composition of subducting sediment and its consequences for the crust and mantle. *Chemical Geology*, **145**, 325–394.

Qian, Q. & Hermann, J. 2010. Formation of high-Mg diorites through assimilation of peridotite by monzodiorite magma at crustal depths. *Journal of Petrology*, **51**, 1381–1416.

Qian, Q., Chung, S.L., Lee, T.Y. & Wen, D.J. 2003. Mesozoic high-Ba–Sr granitoids from North China: geochemical characteristics and geological implications. *Terra Nova*, **15**, 272–278.

Rapp, R.P., Norman, M.D., Laporte, D., Yaxley, G.M., Martin, H. & Foley, S.F. 2010. Continental formation in the Archean and chemical evolution of the cratonic lithosphere: melt–rock reaction experiments at 3–4 GPa and petrogenesis of Archean Mg-diorites. *Journal of Petrology*, **51**, 1237–1266.

Rudnick, R.L. & Gao, S. 2003. Composition of the continental crust. *In*: Rudnick, R.L. (ed.) *The Crust*. Treatise on Geochemistry, **3**, 1–64.

Shimoda, G., Tatsumi, Y., Nohda, S., Ishizaka, K. & Jahn, B.M. 1998. Setouchi high-Mg andesites revisited: geochemical evidence for melting of subducted sediments. *Earth and Planetary Science Letters*, **160**, 479–492.

Steiger, R.H. & Jäger, E. 1977. Subcommission on geochronology; convention on the use of decay constants in geochronology and cosmochronology. *Earth and Planetary Science Letters*, **36**, 359–362.

Stern, R.A., Hanson, G.N. & Shirey, S.B. 1989. Petrogenesis of mantle-derived, LILE-enriched Archean monzodiorites and trachyandesites (sanukitoids) in southwestern Superior Province. *Canadian Journal of Earth Sciences*, **26**, 1688–1712.

Sun, S.S. & McDonough, W.F. 1989. Chemical and isotopic systematics of oceanic basalts: implications for mantle composition and processes. *In*: Saunders, A.D. & Norry, M.J. (eds) *Magmatism in the Ocean Basins*. Geological Society, London, Special Publications, **42**, 314–353.

Tatsumi, Y. 2006. High-Mg andesites in the Setouchi volcanic belt, southwestern Japan: analogy to Archean magmatism and continental crust formation? *Annual Review of Earth and Planetary Sciences*, **34**, 467–499.

Veevers, J.J. 2004. Gondwanaland from 650–500 Ma assembly through 320 Ma merger in Pangea to 185–100 Ma breakup: supercontinental tectonics via stratigraphy and radiometric dating. *Earth-Science Reviews*, **68**, 1–32.

Wang, Q., Liu, X. & Li, J. 1991. *Plate Tectonics Between Cathaysia and Angaraland in China*. Peking University Press, Beijing.

Wang, Y.J., Fan, W.M., Zhang, H.F. & Peng, T.P. 2006. Early Cretaceous gabbroic rocks from the Taihang Mountains: implications for a paleosubduction-related lithospheric mantle beneath the central North China Craton. *Lithos*, **86**, 281–302.

Wenner, J.M. & Coleman, D.S. 2004. Magma mixing and Cretaceous crustal growth: geology and geochemistry of granites in the Central Sierra Nevada batholith, California. *International Geology Review*, **46**, 880–903.

Windley, B.F., Alexeiev, D., Xiao, W.J., Kroner, A. & Badarch, G. 2007. Tectonic models for accretion of the Central Asian Orogenic belt. *Journal of the Geological Society, London*, **164**, 31–47.

Woodhead, J.D., Hergt, J.M., Davidson, J.P. & Eggins, S.M. 2001. Hafnium isotope evidence for 'conservative' element mobility during subduction zone processes. *Earth and Planetary Science Letters*, **192**, 331–346.

Woodhead, J.D., Hergt, J., Shelley, M., Eggins, S. & Kemp, R. 2004. Zircon Hf-isotope analysis with an excimer laser, depth profiling, ablation of complex geometries, and concomitant age estimation. *Chemical Geology*, **209**, 121–135.

Wu, F.Y., Yang, Y.H., Xie, L.W., Yang, J.H. & Xu, P. 2006. Hf isotopic compositions of the standard zircons and baddeleyites used in U–Pb geochronology. *Chemical Geology*, **234**, 105–126.

Xiao, W., Windley, B.F., Hao, J. & Zhai, M. 2003. Accretion leading to collision and the Permian Solonker suture, Inner Mongolia, China: termination of the Central Asian orogenic belt. *Tectonics*, **22**, 1069, doi:10.1029/2002TC001484.

Yang, J.H., Wu, F.Y., Wilde, S.A. & Zhao, G.C. 2008. Petrogenesis and geodynamics of late Archean magmatism in eastern Hebei, eastern North China Craton: geochronological, geochemical and Nd–Hf isotopic evidence. *Precambrian Research*, **167**, 125–149.

Yang, Y.H., Wu, F.Y., Wilde, S.A., Liu, X.M., Zhang, Y.B., Xie, L.W. & Yang, J.H. 2009. *In situ* perovskite Sr–Nd isotopic constraints on the petrogenesis of the Ordovician Mengyin kimberlites in the North China. *Chemical Geology*, **264**, 24–42.

Ye, H.M., Li, X.H., Li, Z.X. & Zhang, C.L. 2008. Age and origin of high Ba–Sr appinite granites at the northwestern margin of the Tibet plateau: implications for early Paleozoic tectonic evolution of the Western Kunlun orogenic belt. *Gondwana Research*, **13**, 126–138.

Zhang, S.H., Zhao, Y., Song, B., Yang, Z.Y., Hu, J.M. & Wu, H. 2007. Carboniferous granitic plutons from the northern margin of the North China block: implications for a late Paleozoic active continental margin. *Journal of the Geological Society, London*, **164**, 451–463.

Zhang, S.H., Zhao, Y., *et al.* 2009*a*. Contrasting late Carboniferous and late Permian–middle Triassic intrusive suites from the northern margin of the North China Craton: geochronology, petrogenesis and tectonic implications. *Geological Society of America Bulletin*, **121**, 181–200.

Zhang, S.H., Zhao, Y., Liu, X.C., Liu, D.Y., Chen, F.K., Xie, L.W. & Chen, H.H. 2009*b*. Late Paleozoic to early Mesozoic mafic–ultramafic complexes from the northern North China Block: constraints on the composition and evolution of the lithospheric mantle. *Lithos*, **110**, 229–246.

Zhang, X.H. & Zhai, M.G. 2010. Magmatism and its metallogenetic effects during the Paleozoic continental crustal construction in northern North China: an overview. *Acta Petrologica Sinica*, **26**, 1329–1341.

Zhang, X.H., Zhang, H.F., Tang, Y.J., Wilde, S.A. & Hu, Z.C. 2008. Geochemistry of Permian bimodal volcanic rocks from Central Inner Mongolia, North China: implication for tectonic setting and Phanerozoic continental growth in Central Asian orogenic belt. *Chemical Geology*, **249**, 261–281.

Zhang, X.H., Zhang, H.F., Jiang, N., Zhai, M.G. & Zhang, Y.B. 2010*a*. Early Devonian alkaline intrusive complex from the northern North China Craton: a petrologic monitor of post-collisional tectonics. *Journal of the Geological Society, London*, **167**, 717–730.

Zhang, X.H., Zhang, H.F., Wilde, S.A., Yang, Y.H. & Chen, H.H. 2010*b*. Late Permian to early Triassic mafic to felsic intrusive rocks from North Liaoning, North China: petrogenesis and implication for Phanerozoic continental growth. *Lithos*, **117**, 283–306.

Zhang, X.H., Mao, Q., Zhang, H.F., Zhai, M.G., Yang, Y. & Hu, Z. 2011*a*. Mafic and felsic magma interaction during the construction of high-K calc-alkaline plutons within a metacratonic passive margin: the early Permian Guyang batholith from the northern North China Craton. *Lithos*, **125**, 569–591.

Zhang, X.H., Wilde, S.A., Zhang, H.F. & Zhai, M.G. 2011*b*. Early Permian high-K calc-alkaline volcanic rocks from northwest Inner Mongolia, North China: geochemistry, origin and tectonic implications. *Journal of the Geological Society, London*, **168**, 525–543.

Zhao, G.C., Wilde, S.A., Cawood, P.A. & Sun, M. 2001. Archean blocks and their boundaries in the North China Craton: lithological, geochemical, structural and *P–T* path constraints and tectonic evolution. *Precambrian Research*, **107**, 45–73.

Zhou, Z.G., Zhang, H.F., Liu, H.L., Liu, C.F. & Liu, W.C. 2009. Zircon U–Pb dating of basic intrusions in Siziwangqi area of middle Inner Mongolia, China. *Acta Petrologica Sinica*, **25**, 1519–1528.

Received 24 May 2011; revised typescript accepted 15 December 2011.
Scientific Editing by Moonsup Cho.